POLITECNICO DI TORINO
Repository ISTITUZIONALE

Cell orientation under stretch: A review of experimental findings and mathematical modelling

(Article begins on next page)

15 May 2024

Review

Cell orientation under stretch: A review of experimental findings and mathematical modelling

Chiara Giverso, Nadia Loy, Giulio Lucci, Luigi Preziosi *

Department of Mathematical Sciences "G.L. Lagrange", Politecnico di Torino, Corso Duca degli Abruzzi 24, Turin, 10126, Italy

ARTICLE INFO

ABSTRACT

The key role of electro-chemical signals in cellular processes had been known for many years, but more recently the interplay with mechanics has been put in evidence and attracted substantial research interests. Indeed, the sensitivity of cells to mechanical stimuli coming from the microenvironment turns out to be relevant in many biological and physiological circumstances. In particular, experimental evidence demonstrated that cells on elastic planar substrates undergoing periodic stretches, mimicking native cyclic strains in the tissue where they reside, actively reorient their cytoskeletal stress fibres. At the end of the realignment process, the cell axis forms a certain angle with the main stretching direction. Due to the importance of a deeper understanding of mechanotransduction, such a phenomenon was studied both from the experimental and the mathematical modelling point of view. The aim of this review is to collect and discuss both the experimental results on cell reorientation and the fundamental features of the mathematical models that have been proposed in the literature.

1. Introduction

The response of cells to mechanical cues started to attract attention in the 1980s, following the study of cardiovascular pathophysiology. In particular, by observing the cellular arrangement in blood vessels, it was found that cells forming the walls of arteries were oriented along specific directions depending on their location. Endothelial cells in the innermost layer, in direct contact with blood flow, tended to be aligned in the axial direction of the vessel (Buck, 1979; White et al., 1983; Wong et al., 1983; Zhao et al., 1995), while smooth muscle cells in deeper layers, e.g., in the intima and in the internal elastic lamina, exhibited a perpendicular or oblique orientation, forming helical-like structures, with cells sometimes disposed at an angle of $20° - 40°$ with respect to the vascular axial direction (Rhodin, 1962; Holzapfel and Ogden, 2009). The pulsatile behaviour of the heart and the arteries, whose cells are constantly exposed to periodic deformations, stimulated the first experimental investigations, with the aim of gaining a deeper understanding of cell mechanosensitivity and orientation in the circulatory system.

In particular, motivated by his own studies on the ex-vivo orientation of cells in aortic walls (Buck, 1979), Buck was the first to examine the response of cells to mechanical cues *in vitro* (Buck, 1980). He seeded a cell population on a rubber plastic substrate which was then cyclically stretched, to mimic the periodic vessel inflation during pulsatile flow. Similarly to cells *in vivo*, he found that nearly 81% of

fibroblasts tended to reorient between 45° and 90° with respect to the stretching direction. These results attracted some interest since they firstly put in evidence, from the experimental point of view, such an alignment behaviour of stimulated cells *in vitro*, paving the way for successive investigations.

Other pioneering works in the same years attempted to analyse the behaviour of vascular cells under periodic stretches of their environment (Wong et al., 1983; Dartsch and Hammerle, 1986; Dartsch and Betz, 1990; Dartsch et al., 1986; Shirinsky et al., 1989; Ives et al., 1986; Sumpio et al., 1988; Terracio et al., 1988). Generally speaking, it was observed that cells exhibited an active response to the exerted stretch by reorienting in specific directions, according to a variably peaked distribution function of orientations. In particular, a preferential orientation almost perpendicular to the stretching direction emerged in most of the preliminary experimental assays.

Later, analogous experiments were repeated by several researchers with many different cell types and tissues subjected to periodic deformations, such as lung tissue (Shikata et al., 2005; Boccafoschi et al., 2007; Iwaki et al., 2009), bladder tissue (Nagatomi et al., 2005), bones (Neidlinger-Wilke et al., 2001; Sato et al., 2005; Nagayama et al., 2012; Matsugaki et al., 2013), esophagus (Cha et al., 2006; Ritchie et al., 2009), neural-like cells (Lin et al., 2020), to cite but a few. Surprisingly, the reorientation behaviour in response to a precise mechanical stimulus appeared to be a common feature to different

---

* Corresponding author.
E-mail addresses: chiara.giverso@polito.it (C. Giverso), nadia.loy@polito.it (N. Loy), giulio.lucci@polito.it (G. Lucci), luigi.preziosi@polito.it (L. Preziosi).
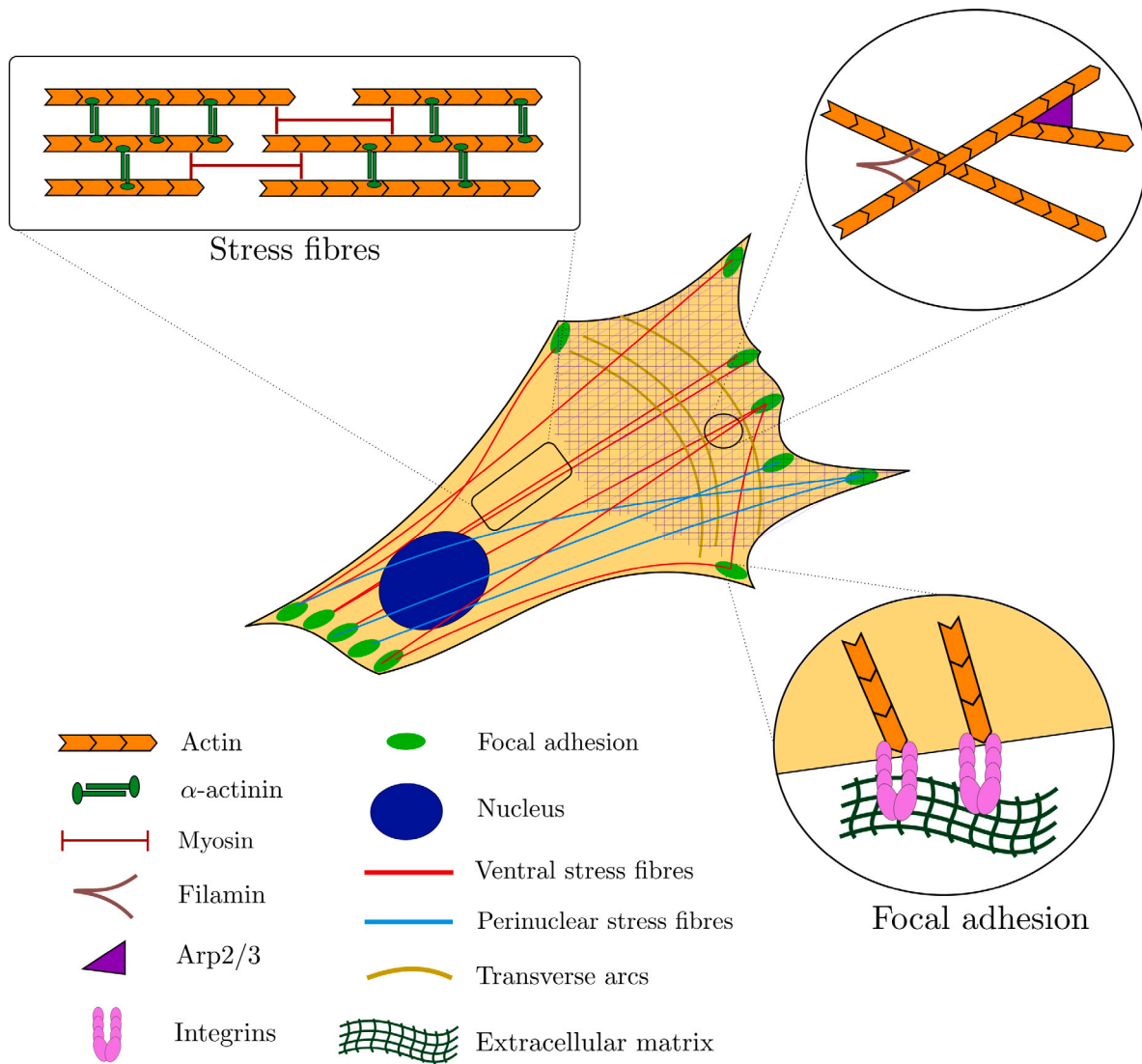
Fig. 1. Sketch of the inner structure of a typical cell and of its adhesion to the substrate.

cell types. As we will discuss later in more detail, epithelial cells, endothelial cells, fibroblasts, osteoblasts, melanocytes, mesenchymal stem cells, in addition to the already cited muscle-type cells, all exhibited reorientation in a similar way.

In such a reorientation process of cells, a key role appears to be played by the cytoskeleton. In particular, among the types of filaments that constitute the typical cytoskeleton of a cell, the *actin stress fibres* (SFs) are probably the most important structure as far as contractility and realignment are concerned. These fibres are composed of actin filaments cross-linked by myosin and other proteins, such as filamin, α-actinin, and the ARP2/3 complex, which behave as bundling structures by linking filaments in parallel or at specific angles (see Fig. 1). In this way, stress fibres are like slender rods crossing the entire cell (Alberts et al., 2008; Tojkander et al., 2012), as sketched in Fig. 1. Stress fibres are also able to actively contract and to develop forces as a response to environmental changes or during cell migration. At the ends of SFs, protein complexes called *focal adhesions* (FAs) connect the cytoskeleton to the external environment, so that the cell is able to sense mechanical changes and to react accordingly. Thus, the interplay of SFs and FAs is crucial in *mechanotransduction*, i.e., the chemical response of the cell to mechanical stimuli. The relevant role of SFs in reorientation, which was firstly highlighted by White et al. (1983) and Wong et al. (1983), was confirmed in subsequent analyses specifically dedicated to

the relationship between periodic stretches and cytoskeletal rearrangement (Hayakawa et al., 2001; Neidlinger-Wilke et al., 2001; Goldyn et al., 2010; Zielinski et al., 2018; Roshanzadeh et al., 2020), as we will discuss extensively in Section 2.1.

Therefore, a common characteristic of mechanically responsive cells seems to be the presence of a robust cytoskeletal architecture and the formation of connected stress fibres and focal adhesions. Furthermore, all the cross-linking molecules mentioned above, as well as actin filaments and adhesion molecules themselves, continuously remodel, leading to cell shape changes and alignment in a specific direction. In particular, when undergoing a periodic stretch, it seems that the reorientation response of a cell and of its cytoskeleton aims at relieving the mechanical discomfort.

Nowadays, a broad range of experimental results about cell reorientation under stretch is available. Indeed, understanding such a process might be of interest in several biomechanical and mechanobiological applications, such as tissue engineering, where the construction of faithful grafts often requires the achievement of a precise cellular organisation. The study of organ development and of pathological degeneration of tissues represents as well an interesting issue, given that disarrangement of cells might be a hallmark of some diseases. Alongside experimental studies, in recent years, there has been an

increasing development of mathematical models attempting to explain the reorientation behaviour of cells.

The aim of this review is then to present both the experimental results and mathematical modelling approaches dealing with cell reorientation phenomena under stretch, in order to collect the available observations and the related modelling frameworks.

In detail, the structure of the paper is the following. Section 2 summarises the experimental findings about cell reorientation and discusses the main features of the experimental assays, as well as the most relevant factors that influence such a behaviour of the cells. Specifically, in Section 2.1 we focus on experiments performed on isotropic, two-dimensional substrates undergoing periodic stretches, both at sub-confluent (Section 2.1.2) and confluent (Section 2.1.3) cell density. With reference to such experimental conditions, we underscore some important characteristics that determine the preferential orientation of a cell, such as the role of the cytoskeleton and the effect of the stretching frequency, amplitude, and substrate stiffness.

Section 2.2 is instead devoted to a summary of experiments performed in three-dimensional structures, like collagen matrices, scaffolds, or artificial constructs built for tissue engineering purposes. In these kinds of structures, in fact, the realignment behaviour of cells appears to be different, because contact guidance comes into play and competes with strain or stress avoidance.

Then, in Section 3 we review the mathematical models proposed in the literature to describe the cell reorientation process under cyclic stretching. We discuss several approaches and classify them according to the main relevant features employed in the model. Finally, in Section 4 we draw some conclusions and outline the open problems, both on the experimental and on the modelling sides.

2. Review of phenomenological observations

2.1. Cells over a two-dimensional substratum

As mentioned above, the results found in some experimental settings almost forty years ago showed evidences that (Buck, 1980; White et al., 1983; Wong et al., 1983; Dartsch and Hammerle, 1986; Dartsch et al., 1986; Shirinsky et al., 1989; Ives et al., 1986; Sumpio et al., 1988; Terracio et al., 1988):

1. In addition to chemical substances, cells appeared to be prone to a response to mechanical cues coming from the environment.
2. The cytoskeleton, and especially the actin fibres, were thought to be involved in the cellular response to an externally applied mechanical force.
3. A reorientation towards a certain preferential direction, still not precisely identified, took place if cells on a substrate were subjected to a cyclic deformation.

Starting from these cornerstones, in the last three decades several attempts to unveil the mechanisms underlying cell alignment and reorientation were performed. Advances in imaging techniques and atomic force microscopy consistently improved the experimental precision, allowing to obtain quantitative measurements of forces, as well as detailed and high-resolution pictures of cellular and sub-cellular structures. These improvements in experimental instruments shed light on some relevant common features about the cellular response to external mechanical stimuli.

Before reviewing the phenomenological findings obtained in more recent years, we discuss some general features of typical experimental set-ups, so as to facilitate a comprehensive understanding of biological experiments and their outcomes.

The two-dimensional settings that are typically used to test the behaviour of cells under stretch consist of a silicon (Hayakawa et al., 2000; Morioka et al., 2011; Hsu et al., 2009; Lee et al., 2010; Ngu et al., 2010; Wang et al., 2001) and/or polydimethylsiloxane (PDMS) substrate (Roshanzadeh et al., 2020; Moretti et al., 2004; Greiner

et al., 2013; Goldyn et al., 2010; Mao et al., 2021), very often coated with collagen or fibronectin to favour cell attachment. Cells are then seeded on the membrane at a certain density and, after attachment, the substrate is pulled along one or two perpendicular directions, either statically or periodically with different waveforms. In most of the experiments, a cyclic stretch in only one direction is applied, as this is the case that probably attracted more interest in clinical applications. Indeed, a uniaxial periodic deformation physiologically happens in several situations: aside from the already cited blood vessels, a number of different tissues and organs undergo periodic strains in physiological conditions, such as the lungs, muscles and tendons, the bladder, and the intestine, to cite but a few.

In general, since the substrate is elastic, a simple pulling of its two lateral sides would naturally lead to a contraction in the perpendicular direction, as shown in Fig. 2(a). In these cases, experimental data are usually reported for those cells in the central portion of the specimen, highlighted in the left panel of Fig. 2(a), where it can be reasonably assumed that stress and strain are homogeneous, with principal directions along the axis of deformation and the orthogonal one. Nevertheless, as we will shortly discuss, the compression of lateral sides relevantly affects the cellular orientation and is one of the main factors that determines the final placement of a mechanically stimulated cell.

In describing the deformation, we will denote by x the direction characterised by the maximum applied stretch. This direction will be also referred to as the *main stretching direction* in what follows. We will then denote by $\varepsilon_{xx}(t) > 0$ and $\varepsilon_{yy}(t)$ the strains along x and y, respectively, and by $\varepsilon_0 := \max_{t \in \mathcal{T}} \varepsilon_{xx}(t)$ the maximum applied strain over the time interval $\mathcal{T}$ of the experiment. Another important quantity that is introduced in the literature and that will be relevant in the mathematical modelling is the so-called *biaxiality ratio*, defined as

$$r := -\frac{\max_{t \in \mathcal{T}} \varepsilon_{yy}(t)}{\max_{t \in \mathcal{T}} \varepsilon_{xx}(t)} = -\max_{t \in \mathcal{T}} \frac{\varepsilon_{yy}(t)}{\varepsilon_0} \, . \tag{1}$$

In static conditions, the parameter r represents the percentage of contraction in the y-direction with respect to the extension applied in the x-direction. If the deformation is uniaxial, as in Fig. 2(a), then r can be identified with the Poisson ratio of the elastic material constituting the substrate.

To avoid the central narrowing of the substrate due to the Poisson effect, some countermeasures have been adopted in experimental works, like thickening the borders parallel to the main stretching direction (as done, for instance, in the work by Dartsch et al., 1986) or attaching the horizontal sides to a more rigid structure or substratum. When these borders are fixed as in Fig. 2(b), then $\varepsilon_{yy} = r = 0$ and it is said that the specimen undergoes a *pure uniaxial stretching*.

The uniaxial settings described so far do not allow to have a full control on the deformation along the vertical axis, which instead may be relevant in determining the cellular orientation, as we will discuss later in more detail. To perform broader and more complete experiments, *biaxial tests* – represented in Fig. 2(c) – that allow to control both strains in the monolayer plane are sometimes performed (Kim et al., 1999; Livne et al., 2014; Liu et al., 2008). In fact, for biaxial experimental settings, r becomes an externally controlled parameter. However, most of the results presented in the literature do not rely on this kind of mechanical stimulus. The only biaxial case which is investigated in several papers is the *equi-biaxial* deformation, where the tensile strains along the x and y directions are equal to each other (Hsu et al., 2009, 2010; Kaunas et al., 2006; Throm Quinlan et al., 2011; Wang, 2000; Wang et al., 2001). However, such a situation is less interesting from the experimental viewpoint, since it does not trigger the reorientation of cells on a substrate, as put in evidence in all the mentioned references.

Whichever type of deformation is considered, most of the experiments are performed with values of $r \in [0, 1]$. We remark however that a negative value of r can be obtained if the substrate is pulled in both directions, as in Kim et al. (1999) and Liu et al. (2008). In particular,
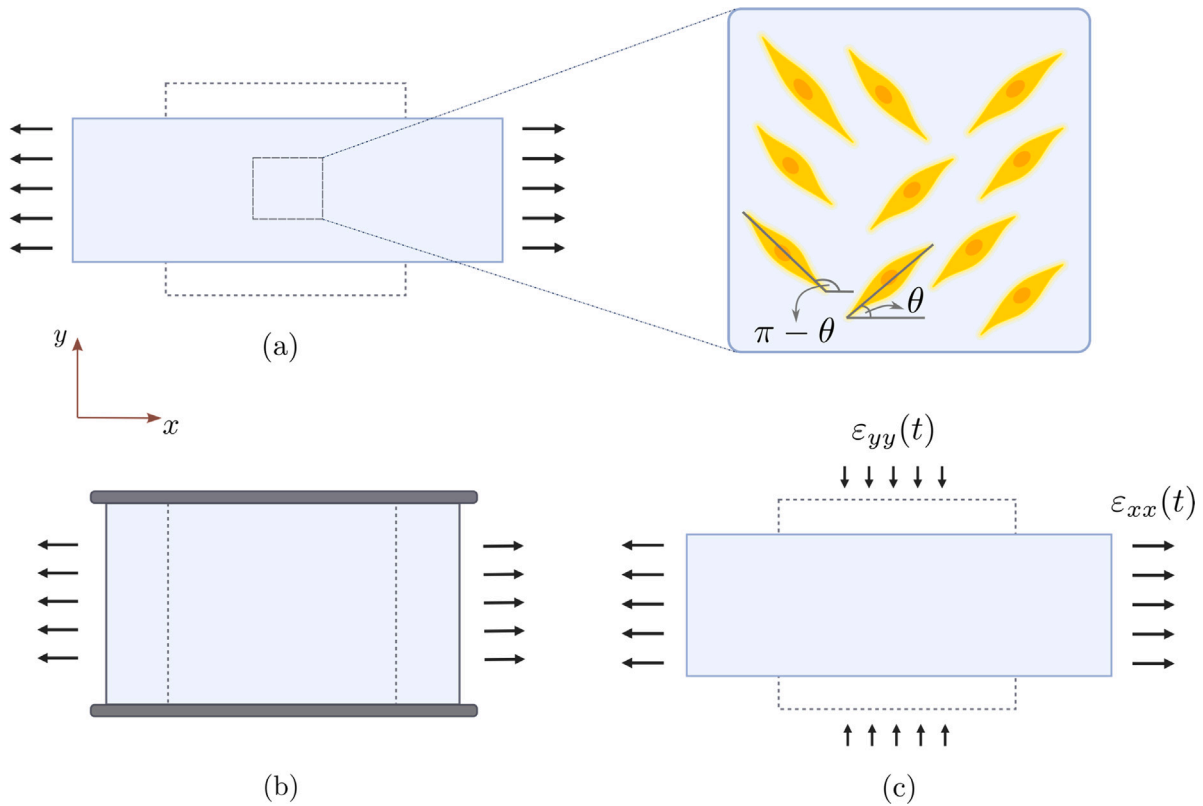
Fig. 2. Sketch of typical experimental set-ups for testing cell reorientation on planar substrates. (a): in uniaxial stretching experiments, the substrate is pulled on two sides, while the other two are free to move inwards following the elasticity of the material. In order to observe a homogeneous deformation applied to cells, only a small central region is examined. The angle between the cell major axis and the main stretching direction is denoted by θ. (b): pure uniaxial stretching experiment, in which two sides of the specimen are clamped to avoid deformation in the vertical direction. (c): biaxial experiments, where the strains are controlled in two directions.

equi-biaxial extension corresponds to $r = -1$. At the other extremum, a value larger than 1 corresponds to a compression along y larger than the pulling along x, which, to our knowledge, has not been done in experiments yet.

As done in the preliminary investigations discussed above, the majority of experiments focus on periodic deformations applied to the substrate, to represent the physiological pulsations *in vivo*. In particular, sinusoidal waveforms defined as

$$\varepsilon(t) = \frac{1}{2}\varepsilon_0\left[1 - \cos(\omega t)\right] = \frac{1}{2}\varepsilon_0\left[1 - \cos(2\pi f t)\right] \qquad (2)$$

are often adopted (see for instance Jungbauer et al., 2008; Mao et al., 2021), in which ε_0 is the maximum amplitude, ω is the angular frequency in rad/s and $f = \frac{\omega}{2\pi}$ is the frequency in Hz, related to the period by $T = 1/f = 2\pi/\omega$ s. Alternatively, triangular (Tondon et al., 2012; Wille et al., 2004; Ngu et al., 2010) or trapezoidal (Tondon et al., 2012; Nagayama et al., 2012; Ritchie et al., 2009; Matsugaki et al., 2013) waveforms might be employed in some cases.

In the following, we introduce the main quantities used for the statistical description of experimental results, before discussing in detail the two-dimensional experiments, both in sub-confluent and confluent conditions. A summary of these experiments, which includes the available characteristics of the assay, the cell type, and the references, can be found in Tables 1–3. We remark that, in the following, we will only consider experiments performed on isotropic, smooth substrates. For experiments that use patterned or micro-grooved surfaces, we refer the reader to the review article by Tamiello et al. (2016).

### 2.1.1. Statistical description of experimental results

Since most of the experimental papers refer to the orientation angle θ of the cell, which is the most natural variable to work with, it is appropriate to firstly comment on the type of data that is usually

reported. In particular, almost all investigators define θ as the angle between the cellular stress fibres (or body) and the main stretching direction, as sketched in Fig. 2(a). This appears to be the simplest way of defining the orientation of a cell, as well as the most effective. However, it is worth to remark that cell orientation experiments present some natural and intrinsic symmetries concerning the angle of alignment. In fact, there is no reason why the cell should prefer the orientation $\pi - \theta$ instead of the one characterised by the angle θ. In addition, as cells do not own a polarisation in the context of reorientation, the angles θ and $\pi + \theta$, as well as $-\theta$ and $\pi - \theta$, turn out to be all equivalent to each other as preferential orientations, as depicted schematically in Fig. 2(a). Such symmetries are evident in a wide number of experimental reports (Dartsch and Betz, 1990; Kanda and Matsuda, 1993; Lin et al., 2020; Livne et al., 2014; Takemasa et al., 1997; Wang et al., 1995; Wang and Grood, 2000; Zhang et al., 2008).

Data are usually given in terms of histograms like those reported in Figs. 4 and 3(b), with most articles reporting orientations in the interval $[0, \pi/2]$ due to the above symmetries. Indeed, in $[0, 2\pi]$, the distribution function of orientations would exhibit four symmetric peaks as in Fig. 3(a).

In this context, it is worth to mention that some experimental papers summarise the data about the angle by computing the mean of the alignment distribution over the all sample of cells. However, we advise that such a measure may be misleading and does not convey much information about the preferential orientation of a cell, in general. Indeed, looking for instance at the histogram in blue in Fig. 3(b), the mean of such a distribution is close to 0, which is far from precise on describing the arrangement of cells. On the other hand, if orientations with negative and positive angles are merged as in the distribution in orange, then the mean will probably be nearby the maximum of the distribution and closer to the preferential direction of cells. In addition, for control samples where cell orientations are
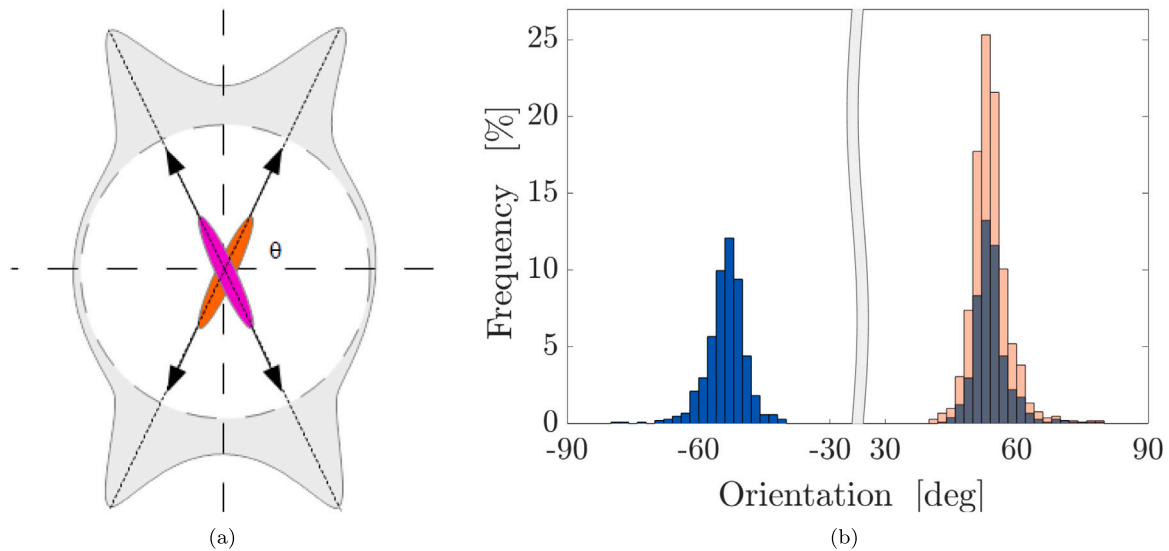
Fig. 3. (a): Example of symmetric distribution of orientations plotted in a polar chart (in grey), with 4 symmetric maxima in $[0, 2\pi]$. (b): Distribution function of cell orientation from data by Livne et al. (2014) when plotted in $\left[-\frac{\pi}{2}, \frac{\pi}{2}\right]$ in blue and when merged in $\left[0, \frac{\pi}{2}\right]$ in orange. Notice the break of the orientation axis between -30 degrees and 30 degrees.

almost uniformly distributed, the mean would trivially be around 45° (see for instance Kanda and Matsuda, 1993; Matsugaki et al., 2013; Yoshigi et al., 2003; Lee et al., 2008; Deibler et al., 2011; Abbott et al., 2012; Standley et al., 2002), which may be misunderstood if not contextualised properly.

For all these reasons, when considering the preferential orientation of cells, in the following we will refer to the peak of the distribution function (or the mode, in statistical terms) rather than the mean, whenever possible or having the experimental data available.

Given the possible shortcomings of a quantitative description based only on the mean orientation angle, different parameters have been employed in the experimental literature, which we briefly summarise below. A useful concept that is often used to measure cell orientation in experimental papers is the *order parameter* (Greiner et al., 2013; Jungbauer et al., 2008; Greiner et al., 2015; Tondon et al., 2012; Tondon and Kaunas, 2014)

$$S := \int_0^\pi g(\theta) \cos 2\theta \, d\theta = \langle \cos 2\theta \rangle, \tag{3}$$

where $g(\theta)$ is the empirical distribution function of cell angles. Hence, a random orientation of the sample corresponds to $S = 0$, whereas a fully coherent parallel orientation gives $S = 1$ and a fully perpendicular one amounts at $S = -1$. However, unless the distribution function is a deterministic Dirac delta, it is not straightforward to relate this parameter with the mode. In other words, although the order parameter S provides a more meaningful measure of the orientation, it does not give a detailed overview of the preferential direction, unless it corresponds to the parallel or perpendicular one. An oblique orientation, which is found quite often in experimental assays, would not be caught if evaluated using such a parameter.

Another measure of cell alignment that is employed to characterise the dispersion in cell orientation is the *circular variance* (Morioka et al., 2011; Hsu et al., 2009; Kaunas et al., 2005; Matsugaki et al., 2013; Tondon et al., 2012; Kaunas et al., 2006):

$$\mathrm{CV} := 1 - \frac{1}{N} \sqrt{\left(\sum_{i=1}^N \sin 2\theta_i\right)^2 + \left(\sum_{i=1}^N \cos 2\theta_i\right)^2}, \tag{4}$$

ranging from 0 to 1. The meaning of such parameter can be easily understood if each cell is associated with a unit vector $\mathbf{N}_i$ of coordinates $\mathbf{N}_i = (\cos\theta_i, \sin\theta_i)$, $i = 1, \ldots, N$. The angles are doubled to account for the symmetry in the direction of the vectors, leading to the same

cellular orientation as described previously. Then, the square root in Eq. (4) represents the length of the vector obtained by summing all the orientations $\mathbf{N}_i$ of the cells in the experiment. It follows that, if the distribution is uniform and totally random, then $\sum_i \mathbf{N}_i \approx \mathbf{0}$ and CV = 1, i.e. the circular variance is maximised. On the other hand, a perfectly aligned cell population will be characterised by the same orientation vector $\mathbf{N}_i = \mathbf{N}$ for all $i = 1, \ldots, N$, leading to CV = 0. In some works, the parameter $R := 1 - \mathrm{CV}$ is instead employed, following the same ideas but with an opposite meaning for the extreme values.

2.1.2. Sub-confluent cells on 2D isotropic substrates

In the majority of experiments on two-dimensional substrates, cells are seeded on the membranes at a sub-confluent density, so that the effect of cell–cell contact and interaction is minimised. Confluent conditions, in which cells get into contact and interact, will be reviewed in Section 2.1.3.

Generally speaking, it is found that, under certain conditions that will be discussed in more detail in the following Subsections, when the specimen is subject to oscillatory deformations there is a reorganisation of the structure of the cytoskeleton that leads to alignment in a precise direction. In addition, the cell acquires an elongated and clearly oriented morphology (Roshanzadeh et al., 2020). Such a behaviour is evident in Fig. 5, which shows some examples of reoriented cells that visibly align along a preferential direction.

In Tables 1 and 2 we summarise the experimental contributions investigating cell reorientation on flat isotropic substrates in sub-confluent conditions. For each experimental test, we report the relevant parameters (or ranges of parameters in square brackets) characterising the assay, as well as the observed preferential orientation, whenever available. With regard to the latter, we remark that, in some works, the final configuration of cells is simply referred to as "perpendicular" or "nearly perpendicular", though the observed angle might be oblique. In the Tables we put in evidence this qualitative description by using the symbol ⊥ (or ≈⊥), at variance with those cases where angles can be more precisely specified thanks to the presence of plots and histograms.

As a first important remark, we observe that several cell types exhibit a reorientation response to periodic strains. Moreover, reorientation appears to some extent almost independent of the applied frequency, amplitude, and of the mechanical characteristics of the substrate. However, in the Tables, we also highlight the values of stretching frequency and amplitude that did not lead to a clear alignment of cells.

Table 1

Summary of the main experiments performed on planar substrates with sub-confluent cells. For each experiment, in addition to the cell type, we report the tested frequencies, amplitudes, biaxiality ratios (whenever available) and preferential orientation. In particular, we use parentheses to address attempted values which however did not give rise to cell reorientation. Instead, square brackets are used to denote a range of values. Abbreviations: N/A = data not available; SMCs = smooth muscle cells; ECs = endothelial cells; MSCs = mesenchymal stem cells; (b) = bovine; (h) = human; (r) = rat; (m) = mouse. We denote by $\perp$ an overall perpendicular orientation, though the precise angle is not specified.

Sub-confluent cells on substrates					
Cell type	f (Hz)	ε_0 (%)	r	θ_{eq} (max)	Refs.
(r) aortic SMCs	0.067	[20, 35]	N/A	$\approx 90°$	Buck (1983)
(r) aortic SMCs	1	20	0.4	[50°, 70°]	Hayakawa et al. (2000, 2001)
(r) aortic SMCs	(0), [0.5, 2]	14	−0.36	[75°, 90°]	Liu et al. (2008)
(b) aortic SMCs	0.25, 1, 2	5, 10, 20	N/A	[80°, 90°]	Kanda and Matsuda (1993)
(h) aortic SMCs	1	10	N/A	[60°, 70°]	Zhu et al. (2011)
(h) umbilical artery SMCs	1	7	N/A	[80°, 90°]	Bono et al. (2016)
(h) bronchial SMCs	0.5	20	0.15	[65°, 70°]	Morioka et al. (2011)
(h) lung alveolar ECs	0.3	5, 10, 15	0.49	76°	Roshanzadeh et al. (2020)
(h) saphenous vein ECs	1	up to 24%	N/A	$\perp$	Iba and Sumpio (1991)
(h) umbilical vein ECs	0.5	10	< 0.3	[80°, 90°]	Yoshigi et al. (2003)
(h) umbilical vein ECs	1	10	N/A	[85°, 90°]	Moretti et al. (2004)
(b) aortic ECs	(0.01), 0.1, 1	10	N/A	$\perp$	Hsu et al. (2009)
(b) aortic ECs	1	(1), [3,10]	0.05	$\perp$	Kaunas et al. (2005)
(h) aortic ECs	0.5	5, 10	N/A	72° (median)	Ngu et al. (2010)
(h) aortic ECs	0.25, 0.5, 1	5, 10	0	[80°, 85°]	Wang et al. (2001)
(h) aortic ECs	0.25, 0.5, 1	5, 10	0.34	[65°, 70°]	Wang et al. (2001)
(h) aortic ECs	0.5	10	0	[80°, 85°]	Wang et al. (2000)
(h) aortic ECs	[0.5, 5]	[2, 10]	0	[63°, 86°]	Wille et al. (2004)
(b) aortic ECs, fibroblasts	1	5	N/A	[80°, 90°]	Kanda and Matsuda (1993)
(b) adrenal cortex ECs	1	10	N/A	[60°, 90°]	Thodeti et al. (2009)
(h) skin fibroblasts	1	4, 8, 12	N/A	$\approx 60°$	Wang and Grood (2000)
(h) skin fibroblasts	1	(0), 4, 8, 12	0.38	[80°, 85°]	Neidlinger-Wilke et al. (2001, 2002)
(m) embryonic fibroblasts	[0.1, 3]	8	0.194	$\perp$	Goldyn et al. (2010), Greiner et al. (2013)
(m) embryonic fibroblasts	(0.01), 0.1, 1	10	0	$\perp$	Hsu et al. (2010)
(r) embryonic fibroblasts	4	8	0.194	67.4° (mean)	Deibler et al. (2011)
(m) fibroblasts	1	5, 10	≈ 0	[100°, 110°]	Chatterjee et al. (2022)
(m) L strain fibroblasts	0.067	N/A	N/A	[45°, 90°]	Buck (1980)
(h) vaginal fibroblasts	0.1	10	N/A	$\perp$	Wang et al. (2015, 2018)
(h) lung fibroblasts	[0.25, 3]	(< 1); [2, 25]	N/A	[60°, 90°]	Boccafoschi et al. (2007)
(h) cortical bone osteoblasts	1	[0, 12]	0.38	[75°, 85°]	Neidlinger-Wilke et al. (2001)
(m) bone osteoblasts	0.5, 1	8	0.52	[40°, 80°]	Nagayama et al. (2012)
(h) osteosarcoma	(0.01), 1	10	$\approx 0, (−1)$	$\perp$	Lee et al. (2010), Hsu et al. (2010)
(h) annulus fibrosus cells	1	10, 15, 20	N/A	86.4° (mean)	Abbott et al. (2012)
(r) bone marrow MSCs	1	10	0.38	[70°, 80°]	Zhang et al. (2008)
(h) bone marrow MSCs	(0), 1.2	10	N/A	64°	Goli-Malekabadi et al. (2011)
(h) bone MSCs	$[3 \cdot 10^{-5}, 2]$	(1); [2, 10]	0	[80°, 100°]	Mao et al. (2021)
(h) melanocytes	1	4, 8, 12	0.38	[55°, 60°]	Wang et al. (1995)
frog epithelial renal cells	1	20	0.4	Oblique	Hayakawa et al. (2001)
(m) neuron-like cells	0.05, 0.15, 0.25	(2), 5, 10	0	[60°, 90°]	Lin et al. (2020)

Table 2
Summary of the main experiments performed on planar substrates with specified mechanical characteristics in sub-confluent conditions. In particular, for each experiment we report the Young modulus E of the substratum, in addition to the other mechanical variables. Abbreviations: N/A = data not available; SMCs = smooth muscle cells; ECs = endothelial cells; MSCs = mesenchymal stem cells; (b) = bovine; (h) = human; (r) = rat; (m) = mouse. We denote by $\perp$ a perpendicular orientation and by $\parallel$ an overall parallel orientation, though the precise angle is not specified.

Sub-confluent cells on substrates with specified Young modulus						
Cell type	f (Hz)	ε_0 (%)	r	E (kPa)	θ_{eq} (max)	Refs.
(h) coronary artery ECs	$(0.01), 0.1, 1$	8	0.194	1000	$\perp$	Greiner et al. (2015)
(h) coronary artery SMCs	$(0.01, 0.1), 1$	8	0.194	1000	$\perp$	Greiner et al. (2015)
(h) umbilical vein ECs	1	10	0.45	900	$[55°, 60°]$	Barron et al. (2007)
(h) umbilical vein ECs	0.13	14	0.5	50	78°	Zielinski et al. (2018)
(h) dermal fibroblasts	$[0.0001, 20]; (< 0.1)$	$(< 2); [3, 16]$	0.194	1000	$\perp$	Jungbauer et al. (2008)
(r) embryonic fibroblasts	$[0.0001, 20]; (< 0.01)$	$(< 1); [2, 16]$	0.194	1000	$\perp$	Jungbauer et al. (2008)
(r) embryonic fibroblasts	$[1.2, 12]$	$[4, 24]$	$[0, 1]$	20,1000	$[45°, 90°]$	Livne et al. (2014)
(h) umbilical cord fibroblasts	$(0), [0.009, 0.052]$	$(0); [4.9, 32]$	0.15, 0.29	$(< 3); 11, 50$	$[65°, 85°]$	Faust et al. (2011)
(h) osteosarcoma	$(0.01), 0.1, 1$	10	0.19, 0.43	$\begin{cases} \text{stiff} \\ \text{soft} \end{cases}$	$\begin{cases} \perp \\ \parallel \end{cases}$	Tondon et al. (2012), Tondon and Kaunas (2014)
(h) MSCs	1	10	0.43	$\begin{cases} \text{stiff} \\ \text{soft} \end{cases}$	$\begin{cases} \perp \\ \parallel \end{cases}$	Tondon and Kaunas (2014)
(m) myoblasts	0.5	7	0.5	≈ 1000	$[60°, 70°]$	Ahmed et al. (2010)
pig valvular interstitial cells	1	10	0	0.9, 150	$\perp$	Throm Quinlan et al. (2011)

Table 3
Summary of the main experiments performed on planar substrates with confluent cells. For each experiment, in addition to the cell type, we report the tested frequencies, amplitudes, biaxiality ratios (whenever available) and preferential orientation. In particular, we use parentheses to address attempted values which however did not give rise to cell reorientation. Instead, square brackets are used to denote a range of values. Abbreviations: N/A = data not available; SMCs = smooth muscle cells; ECs = endothelial cells; MSCs = mesenchymal stem cells; (b) = bovine; (h) = human; (r) = rat; (m) = mouse. We denote by $\perp$ a perpendicular orientation and by $\parallel$ an overall parallel orientation, though the precise angle is not specified.

Confluent cells on substrates					
Cell type	f (Hz)	ε_0 (%)	r	θ_{eq} (max)	Refs.
rabbit aortic SMCs	0.833	$(2), 5$	N/A	$[50°, 60°]$	Dartsch et al. (1986)
rabbit aortic SMCs	0.833	10	N/A	$[70°, 80°]$	Dartsch et al. (1986)
rabbit aortic SMCs	1	$[2, 20]$	N/A	$\approx\perp$	Dartsch and Hammerle (1986)
rabbit aortic SMCs	1	$[2, 20]$	N/A	76° at 15%	Dartsch and Betz (1990)
pig esophageal SMCs	0.0725	2, 5, 10	N/A	$\parallel, \perp, \perp$	Ritchie et al. (2009)
(r) aortic SMCs	1	up to 25%	N/A	$[70°, 80°]$	Standley et al. (2002)
(r) aortic SMCs	1	$[10, 110]$	$[0.32, 0.7]$	$[62°, 68°]$	Takemasa et al. (1998)
pig aortic ECs	1	15	N/A	89°	Dartsch and Betz (1990)
(b) aortic ECs	1	10	≈ 0.05	$\perp$	Kaunas et al. (2005, 2006)
(b) aortic ECs	$(0.01), 0.1, 1$	10	≈ 0	$\perp$	Hsu et al. (2010), Lee et al. (2010)
(h) pulmonary microvascular ECs	0.833	20	N/A	$\perp$	Iwaki et al. (2009)
(h) umbilical vein ECs	0.867	20	N/A	$[80°, 120°]$	Shirinsky et al. (1989)
(h) umbilical vein ECs	0.5, 1, 2	$(0), [10, 110]$	$[0.32, 0.7]$	$[61°, 69°]$	Takemasa et al. (1997, 1998)
(h) umbilical vein ECs	0.5	10	< 0.3	$[80°, 90°]$	Yoshigi et al. (2003)
(h) umbilical vein ECs	1	10	N/A	90°	Ives et al. (1986)
(b) aortic ECs	1	10	N/A	$\perp$	Ives et al. (1986)
(m) osteoblast	$[0.017, 0.17]$	2, 4, 10	0.49	$[50°, 70°]$	Matsugaki et al. (2013)
(r) myocytes, fibroblasts, ECs	0.167	5, 10	N/A	$\perp$	Terracio et al. (1988)
(h) MSCs	1	5	N/A	$\perp$	Kurpinski et al. (2006)
(r) cardiomyocytes	0.5	20	N/A	$[0°, 30°]$	Yamane et al. (2007)
(h) dermal fibroblasts	0.17	20	N/A	$\perp$	Huang et al. (2013)
(h) intestinal cells	0.125	10	0.4	$[70°, 90°]$	Gérémie et al. (2022)
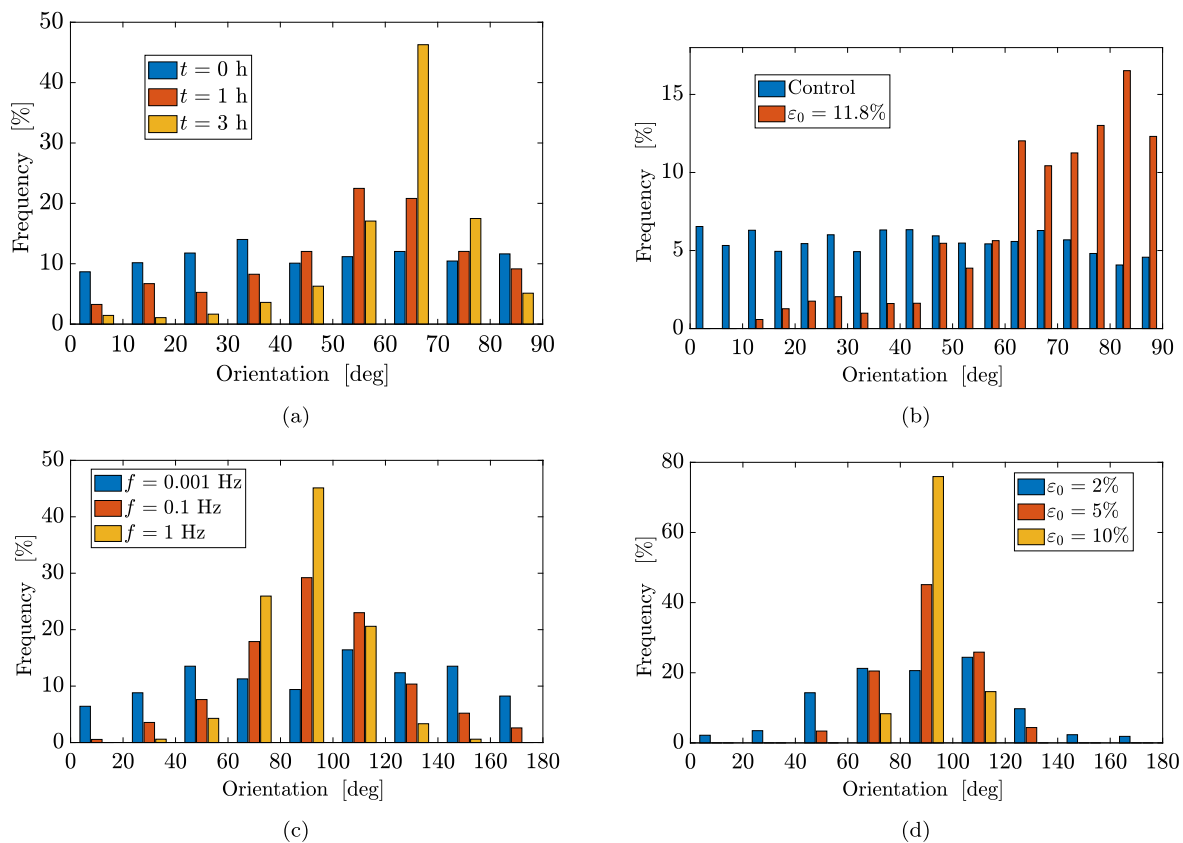
Fig. 4. (a): Temporal evolution of orientation angles for the cell body in experiments by Hayakawa et al. (2000). (b): Distribution of final cell orientation for a maximum strain of 11.8% (in red) compared with the control case (in blue). Data taken from Faust et al. (2011). (c): Distribution of final cell orientation for a maximum strain of 5% at different frequencies, specifically, 0.001 Hz in blue, 0.1 Hz in orange, 1 Hz in yellow. Data taken from Mao et al. (2021). (d): Distribution of final cell orientation for a fixed frequency of 1 Hz and maximum strain of 2% (in blue), 4% (in orange), and 10% (in yellow). Data taken from Mao et al. (2021).

In what follows, the role of biological components – like the cytoskeleton – and of mechanical parameters – like frequency and amplitude of the deformation, as well as substrate stiffness – will be discussed in more detail, with reference to the Tables that summarise the experimental results.

Reorientation of the cytoskeleton

As mentioned previously, the cell cytoskeleton, i.e., the network of protein filaments and structures that is found in the cytoplasm, fulfils a fundamental role in sensing the external mechanical stimuli and in driving the subsequent reorientation towards the preferential direction. One of the first works highlighting the relevance of the cytoskeleton in the realignment process is the one by Hayakawa et al. (2001), who studied the relationship between cytoskeletal rearrangement and cytoplasm reorientation. They put in evidence a significant time difference between the reorientation of SFs and the one of the cell body. The former started after 5 min of stretching and completed within 15 min. Instead, the latter – whose distribution over time is reported in Fig. 4(a) – was more gradual and took up to 3 h. These results about the dynamics of reorientation, with a significant delay between stress fibre and cell body alignment, are supported by several other authors (see, for instance, Hsu et al., 2009; Livne et al., 2014; Moretti et al., 2004; Morioka et al., 2011; Neidlinger-Wilke et al., 2002; Wang et al., 2001). The necessity of SFs for reorientation was also argued: if they were depleted using Cytochalasin B, cell alignment was almost blocked and significantly inhibited.

Neidlinger-Wilke et al. (2001, 2002) provided further evidence supporting the role of the cytoskeleton, since fibroblasts appeared more mechanically responsive in reorientation than osteoblasts. The former indeed have a stronger cytoskeleton than the latter, given that they exert large traction forces on the extracellular matrix (ECM).

Then, a very relevant and detailed analysis of the role of cytoskeletal components on the reorientation kinetics was performed more recently by Goldyn et al. (2010) and by Zielinski et al. (2018). As confirmed by several other investigators, in the work by Goldyn et al. (2010) it was found that actin-disrupting drugs inhibit cellular reorientation, while microtubules (MTs), i.e. another cytoskeletal component, do not appear necessary to achieve cell alignment under cyclic stretching. Such a finding about microtubules is consistent with the observations of several other investigators (Hayakawa et al., 2000; Wang et al., 2001; Greiner et al., 2013; Chatterjee et al., 2022). However, the role of MTs is still debated: Morioka et al. (2011) demonstrated instead that a relevant interplay between microtubules and actin SFs exists and affects the reorientation of the cytoskeleton. Specifically, their findings show that MTs also aligned along the cell axis under a cyclic stretch and, if MTs are disrupted or stabilised with appropriate drugs, cells do not seem to orient effectively. In addition, in the work by Zielinski et al. (2018) all the cytoskeletal structures, including MTs, were found to reorient obliquely or perpendicularly to the main strain direction, with different kinetics. Further investigations are therefore needed to assess the contribution of cytoskeletal structures different from the actin stress fibres, whose role has been elucidated more precisely.

Having established the importance of the cytoskeletal actin architecture in the reorientation process, a very recent work by Roshanzadeh et al. (2020) focused on the mechanoadaptive role of stress fibre subtypes. Indeed, previous experimental analyses concerning the various components of the cytoskeleton were mainly directed to a single type of SFs or MTs, even if, within the cell supporting structure, different types of SFs actually exist, performing different roles. In this regard, the most relevant result of this work lies in the study of the interdependence of different SFs structures. The cytoplasm, whose reorientation was
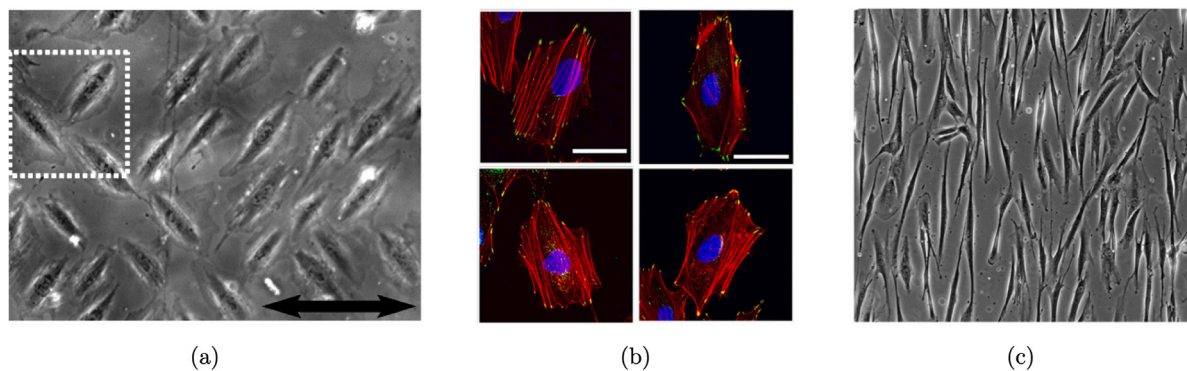
Fig. 5. Microscopic representative examples of reoriented cells under stretch. (a): rat fibroblasts oriented in symmetric directions after 6 h of cyclic stretching at 1.2 Hz and 10% amplitude, with stretching direction highlighted by the double-headed arrows (taken with permission from Livne et al., 2014). (b): human lung alveolar epithelial cells (taken from Roshanzadeh et al., 2020) at different times and stretching amplitudes. The main cell and cytoskeletal components can be identified: actin stress fibres (in red), focal adhesions (in green), and nucleus (in blue). Scale bars: 100 μm. (c): human fibroblasts after 24 h of cyclic stretching at 0.17 Hz and 20% amplitude. Notice that, in this case, cells are almost in confluence and there might be some cell–cell contacts (taken with permission from Huang et al., 2013).

driven by the *peripheral SFs*, oriented at 76° regardless of the strain magnitude, while the nucleus, guided by *perinuclear cap fibres*, showed a lagged dynamics, especially at small strains. The possibly different responsiveness of SFs types to mechanical stimuli was suggested before by Tamiello et al. (2015) in experiments including contact guidance.

To complete the discussion about the cytoskeletal response and consequent reorientation, an interesting result concerns the only counterexample that is reported. Indeed, a cell type that does not appear to respond following a stretch-avoidance mechanism are *immune cells*, like macrophages, neutrophils, or monocytes. This behaviour is probably due to the fact that immune cells do not possess a strong cytoskeleton and they are not able to generate sufficient traction forces (Haston et al., 1983; Harris et al., 1980). Indeed, they have to squeeze while patrolling the body for potential pathogens and exhibit an amoeboid motion, unlike other types of cells. In particular, Matsumoto and coworkers (Matsumoto et al., 1996) found that rat macrophages do not appear to be strongly responsive to an applied mechanical stimulus, while an alignment slightly parallel to the direction of stretch is reported for human monocytes (Matsumoto et al., 1996). This is in contrast with the common behaviour for other cell types, which exhibit an avoidance of cyclic strain and reorient obliquely or perpendicularly to the main stretching direction, as discussed before and summarised in the Tables. Subsequent studies confirmed this behaviour of immune cells (Matheson et al., 2006; Atcha et al., 2018a,b) for cyclic strain at different amplitudes (10% and 20%) and frequencies (0.25 Hz and 1 Hz), both low and high.

In the following Subsections, we will discuss thoroughly the role of mechanical parameters, like the stretching frequency, the stretching amplitude and the substrate stiffness, in the process of cell and stress fibre alignment.

Frequency effect

The natural frequency to test cell behaviour is a physiological value of 1 Hz, corresponding to normal heart beats (Mason et al., 2007), or alternatively a value in the range 0.25 Hz − 0.3 Hz, corresponding to breathing frequency (Takayama et al., 2019). The first work to explore the possibility of differences in cell orientation due to the stretching frequency is the one by Kanda and Matsuda (1993). Although they employed only the mean orientation angle of the cell population to quantify the frequency effects, an increase from 0.25 Hz to 1 Hz and to 2 Hz provoked an increase in such an angle, meaning that the alignment of cells was more pronounced towards the perpendicular orientation. However, as discussed above, providing the mean angle as a measure is not the most effective way to convey the results.

One of the most detailed works concerning the effects of amplitude and frequency is due to Jungbauer and collaborators (Jungbauer et al.,

2008). In their work, a wide range of frequencies is tested on rat embryonic fibroblasts (REF) and human dermal fibroblasts (HDF). The results suggest that there is a cell-type-dependent *minimal threshold frequency* needed to induce a significant cellular reorientation: such a threshold amounts at about 0.01 Hz for REF and 0.1 Hz for HDF. Moreover, a linear log–log relationship between the reorientation time and the frequency is observed: higher frequencies below 1 Hz are associated with a faster process, as clear from Fig. 6(a), and also with a greater alignment of the cellular population, as shown in Fig. 4(c). The most relevant finding however is the existence of an *upper threshold frequency* of approximately 1 Hz, above which the reorientation time saturates and the process cannot be accelerated anymore in sub-confluent populations. More specifically, above a threshold value of 0.5 Hz for REF and 1 Hz for HDF, the reorientation time becomes nearly constant and equal to 80 min for the former and 120 min for the latter (see yellow and red curves in Fig. 6(a)). Below the threshold value, instead, the characteristic time increases and is equal to nearly 3 h in the case of REF for a frequency $f = 0.05$ Hz and about 5 h in the case of HDF for $f = 0.25$ Hz. According to the authors, such a result, which was also confirmed later by another group (Greiner et al., 2013), might be due to the saturation of some molecular mechanism driving the reaction to the stimulus that cannot be faster for periods above 1 s. The hypothesis is corroborated by the results in confluent conditions, where no saturation is observed and the characteristic time is a strictly decreasing function of the applied frequency, as clearly evident from the blue curve in Fig. 6(a). Indeed, for high cellular densities, the cell–cell contacts through cadherins become relevant and may provide an additional sensing machinery that prevents saturation and speeds up the reorientation. It is also worth to observe that, in general, confluent cells reorient faster than sub-confluent layers, as shown by the blue curve in Fig. 6(a). We will discuss such issue in more detail in Section 2.1.3.

The presence of a cell-type-dependent frequency threshold to trigger cell response, pointed out in the work by Jungbauer et al. (2008), appears to be a crucial issue and is confirmed by several experimental reports. For instance, the frequency must be larger than 0.01 Hz for rat embryonic fibroblasts (Jungbauer et al., 2008; Greiner et al., 2013), osteoblasts (Tondon et al., 2012; Lee et al., 2010), and bovine aortic endothelial cells (Hsu et al., 2009; Lee et al., 2010). Instead, the frequency should be above 0.1 Hz for human dermal fibroblasts (Jungbauer et al., 2008), human coronary artery endothelial cells (Greiner et al., 2015) and at least 1 Hz for human coronary artery smooth muscle cells (Greiner et al., 2015). Interestingly, a frequency of 0.05 Hz seems to be enough to induce neuronal alignment away from the stretching direction (Lin et al., 2020). However, these differences with the cell type do not affect the cytoskeletal structures, i.e. stress fibres and
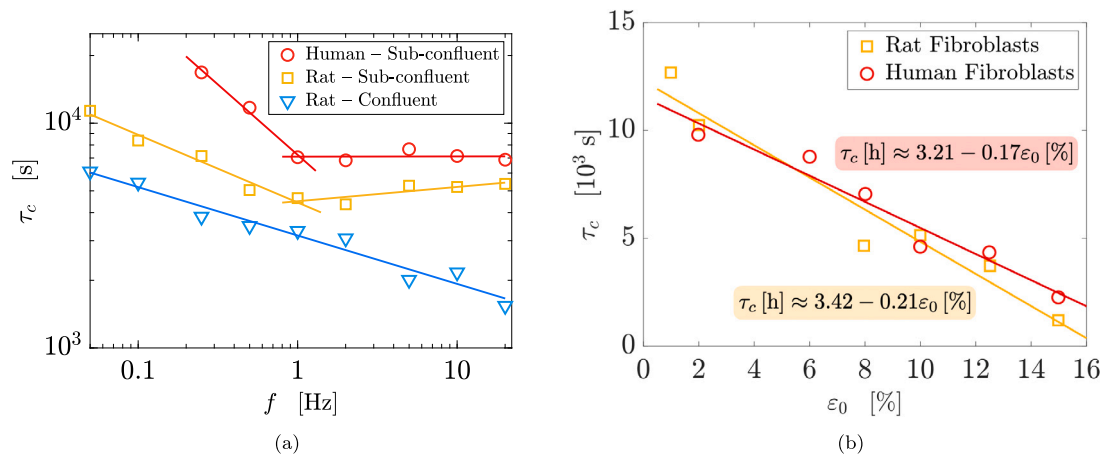
Fig. 6. Experimental relationships for the reorientation time. (a): characteristic time τ_c of reorientation as a function of the applied frequency f, in log–log scale, with data from Jungbauer et al. (2008). In the sub-confluent case, two regimes can be distinguished: a first one in which the characteristic time follows a power law decrease and a second one where, for frequencies above 1 Hz, τ_c remains almost constant. This is not the case for confluent cells, for which the time always decreases with no saturation. (b): characteristic time as a function of the amplitude ε_0.
Source: Data taken from Jungbauer et al. (2008).

focal adhesions, which instead are found to be oriented at 0.1 Hz independently of the cell line (Greiner et al., 2015). Such data support previous findings about the delayed and less sensitive response of the cell body, compared with the mechano-reception of the stimulus by the cytoskeleton.

Very low frequencies in the range of 9–52 mHz applied to human umbilical fibroblasts appeared however to stimulate a cellular reorientation response, though the time span required to observe a steady state was considerably increased (Faust et al., 2011).

An additional consequence of the increase in the cyclic strain frequency is an observed decrease of the circular variance (Hsu et al., 2009), meaning that the distribution of cells on the substrate has become more peaked towards the preferential orientation. Therefore, higher frequencies make cells to align more coherently to avoid strain, as observed in several experiments (Jungbauer et al., 2008; Mao et al., 2021; Hsu et al., 2009; Greiner et al., 2013) and shown in Fig. 4(c). Instead, a different and somehow counter-intuitive result is found by Liu et al. (2008), who showed that the amount of cells oriented perpendicularly decreases with the frequency.

It is worth to separately discuss the results by Mao and collaborators (Mao et al., 2021) about the frequency, which are reported in Fig. 4(c). In addition to observing a more aligned distribution as the frequency increases, the authors found that the minimal frequency necessary to observe a reorientation of cells appeared to be amplitude-dependent. More specifically, higher frequencies were required for the onset of cellular realignment at low amplitudes, suggesting that the action of these two mechanical parameters is not fully decoupled. Thus, the authors propose a single parameter to summarise the frequency–amplitude threshold, which they call *critical stretching rate* and is defined by $\pi f \varepsilon_0$, or equivalently $\frac{1}{2}\omega\varepsilon_0$. The reciprocal of such value, amounting at 8.3 min, correlates well with the turnover time of actin filaments reported in the literature (Mao et al., 2021; Kreis et al., 1982).

Other studies that analyse variations of the strain rate are the ones by Wille et al. (2004), Nagayama et al. (2012), and Tondon et al. (2012), Tondon and Kaunas (2014). In particular, in Nagayama et al. (2012) it is suggested that alignment was mainly promoted by compressive forces acting on the SFs, whereas an opposite mechanism is proposed in Tondon et al. (2012) and Tondon and Kaunas (2014), with greater fibre sensitivity to the lengthening rate. Hence, the role of the strain rate does not appear fully elucidated.

We conclude the discussion about the frequency by considering the possibly relevant case in which the specimen is subjected to a *step stretch*, which is then sustained without oscillations, corresponding to a null applied frequency. In this situation, however, the behaviour of cells is not well clarified. Indeed, if the static stretch is regarded as a limit case of low frequency, one would expect that the sample keeps having a uniform distribution of orientation angles. This is observed in some experimental settings (Liu et al., 2008; Hayakawa et al., 2000; Goli-Malekabadi et al., 2011). On the contrary, a step deformation provoked an alignment parallel with the stretching direction in other works (Tondon et al., 2012; Tondon and Kaunas, 2014; Chen et al., 2013). Interestingly, Tondon and Kaunas (2014) also put in evidence that a static step stretch promoted parallel alignment on soft gels, but not on stiff silicone substrates.

To summarise the results about the role of the frequency, the main experimental findings are the following:

- There exists a lower frequency threshold ω_l, below which no reorientation happens.
- There exists an upper frequency threshold ω_u, above which – in sub-confluent conditions – cell alignment cannot become faster. These thresholds depend on the cell type.
- If the frequency falls between ω_l and ω_u, the effect of an increase is twofold. First of all, the number of cells oriented in the preferential direction increases. Indeed, if ω is low, fewer cells are found to be aligned, while most of the population remains randomly oriented. Conversely, for high frequencies, the probability distribution of oriented cells becomes highly peaked around the preferred orientation angle. Second, higher frequencies are associated with a faster reorientation, and therefore with a lower characteristic time (Jungbauer et al., 2008). These effects emerge visibly in Figs. 4(c) and 6(a).
- The preferential angle at steady state, at least according to some experimental works, does not seem to be affected by a change in the frequency, provided that the latter is above the minimal threshold ω_l (Faust et al., 2011; Niediek et al., 2012; Mao et al., 2021; Tondon et al., 2012).
- There might be a combined action of frequency and amplitude in determining the thresholds ω_l and ω_u and therefore the onset of cell alignment, with higher amplitudes required at low frequencies and vice versa.

Amplitude effect

As for the frequency, a minimal strain amplitude needs to be applied in order to induce cell reorientation. Such threshold is generally in the range of few percent of substrate strain. For instance, an amplitude

of at least 1% was needed for fibroblasts (Boccafoschi et al., 2007; Jungbauer et al., 2008), 3% for bovine aortic endothelial cells (Kaunas et al., 2005), 4.4% for human bone mesenchymal stem cells (Morita et al., 2013), and 5% for neural-like cells (Lin et al., 2020). A similar behaviour is also seen in confluent conditions where, for instance, a strain of at least 2% was needed (Dartsch et al., 1986) to reorient rabbit arterial smooth muscle cells. As discussed before, Mao et al. (2021) recently observed that the minimum amplitude value decreases for increasing frequencies. This is not surprising, as both of them have the effect of promoting reorientation and lead to more peaked distribution functions, as shown in Figs. 4(c)–4(d).

Although the amplitude of the cyclic stretch does not seem to alter the preferential orientation of the stress fibres (Roshanzadeh et al., 2020; Takemasa et al., 1997, 1998), it determines the degree of alignment of the cellular population, with higher amplitudes causing a decrease in the circular variance (Kaunas et al., 2005; Hsu et al., 2009) and therefore a more coherent and pronounced orientation towards the preferential direction (Hsu et al., 2009; Kanda and Matsuda, 1993; Faust et al., 2011; Standley et al., 2002). Moreover, an increase in amplitude above the lower threshold apparently causes a decrease in the characteristic reorientation time. For instance, as shown in Fig. 6(b), Jungbauer and coworkers (Jungbauer et al., 2008) report data showing a linear negative correlation between the reorientation time and the magnitude of applied strain. The fitting suggests an almost linear decrease, in the range of strain considered, with $\tau_c \approx 3.21 - 0.17\varepsilon_0$ hours for human fibroblasts and $\tau_c \approx 3.42 - 0.21\varepsilon_0$ hours for rat embryonic fibroblasts when $\varepsilon_0 < 16\%$. Therefore, unlike the frequency case, in the tested range of amplitudes no saturation is observed as ε_0 increases, though it can be expected at very large strain amplitudes. Of course, a maximum strain bearable by cells also exists, because cell injuries, detachments, and even death may occur if the deformation is too large. For instance, amplitudes greater than 25% might be harmful for the cell population on the substrate (Boccafoschi et al., 2007). However, some of the most detailed results in terms of cell orientation obtained by Livne et al. (2014) and Faust et al. (2011) apply strains of 24% and 32%, respectively. The maximum applied strain in the experiments by Standley et al. (2002) reaches 25% with no reported damage, while Takemasa and coworkers (Takemasa et al., 1998) even employed a 110% strain with their experimental device. Hence, the maximum deformation that can be sustained by a cell might be dependent on its type and also on the mechanical properties of the substrate.

In summary, the effects of the cyclic strain amplitude on the reorientation of cells and SFs are as follows:

- There exists a minimum amplitude necessary to induce a reorientation response. Such a lower threshold appears to be cell-type dependent and probably also frequency-dependent according to recent results (Mao et al., 2021).
- An increase in amplitude leads to a faster reorientation of cells away from the stretching direction (Jungbauer et al., 2008), as in Fig. 6(a).
- Greater amplitudes are associated with a more peaked orientation of the cell population along the preferential direction, as in Fig. 4(d).

Substrate stiffness effect

As mentioned in Table 1, most of the experiments do not characterise the substrate from the mechanical point of view. In the majority of cases, silicon or polydimethylsiloxane (PDMS) are used, usually coated with collagen or fibronectin to favour cell attachment and mimic the ECM composition. However, as shown by Moretti et al. (2004), reorientation happens also on engineered silicone substrates without precoating, meaning that the cell response might be independent of any external adhesion promoter. The elastic modulus of the materials employed as substrates is often close to 1 MPa, making them quite stiff and almost impossible to be deformed by cellular traction forces.

On the other hand, the experiments cited in Table 2 report the mechanical characteristics of the substratum and some of them focus

on what happens when softer materials are used. In particular, as a consequence of substrate softening, the externally applied strain is not completely transferred to the cells attached to its surface. Differently, for stiff environments it is sometimes stated that all the strain is also transferred to the cell (Neidlinger-Wilke et al., 2001, 2002). However, Tondon and Kaunas (2014) report a difference of 4% between the two. In the experiments performed by Wille et al. (2004) and Wang et al. (2001), instead, only 77% of the strain of the substrate was actually transmitted to the cell.

Changes in substrate stiffness are also investigated in the work by Faust et al. (2011). Specifically, cells seeded on very soft substrates, with Young moduli of 1–3 kPa, did not respond to cyclic stretches at all. A first, significant reorientation of actin bundles is observed for 11 kPa of substrate rigidity, meaning that a possible stiffness threshold between 3 and 11 kPa exists to induce cell reorientation. According to the authors, for low values of substrate Young modulus, the mechanosensitive apparatus of human umbilical cord fibroblasts was not well established, and so cells were not able to effectively respond to the applied strain.

Conversely, Tondon et al. (2012) showed that osteosarcoma epithelial cells and mesenchymal stem cells tend to orient preferentially along the stretching direction, i.e. $\theta_{eq} = 0°$, on softer thick collagen gels, while the perpendicular alignment is still found on stiffer collagen-coated silicone substrates (values of Young modulus not explicited, but probably of the order of 1 MPa). Interestingly, such results are consistent with a previous study (Kaunas et al., 2005) where SFs in cells with reduced contractility due to treatment with specific inhibitors were found to align parallel to the stretching direction as well. Attenuated contractility may also be a relevant factor in cells adhering to soft substrates, which display a reduced number of SFs (Tondon et al., 2012).

Livne et al. (2014) instead did not find significant differences in cell preferential orientations when the substrate stiffness is changed from 1 MPa down to 20 kPa. The parameters they estimate appear rather robust with respect to changes in the mechanical properties of the substrate.

The combination of effects due to cyclic stretch and substrate stiffness was investigated by Quinlan and coworkers (Throm Quinlan et al., 2011). Concerning orientation, cells on very soft substrates ($E \approx 0.9$ kPa) showed significantly less alignment than those on stiff substrates ($E \approx 150$ kPa), in accordance with other works.

We also mention that Takemasa and coworkers (Takemasa et al., 1997, 1998) ruled out the influence of substrate coating (fibronectin, collagen, laminin, vitronectin) on the cell preferential angle.

To summarise, we have the following features for the effect of substrate stiffness on cell orientation:

- For cells seeded on stiff substrates, the cell preferential angle seems to be independent of the substrate stiffness.
- Cells on softer substrates appear less prone to respond to mechanical deformations.
- A possible threshold at very low substrate stiffness (e.g., less than 11 kPa) might exist to induce cell reorientation under cyclic stretching.

2.1.3. Confluent cells on 2D isotropic substrates

So far, we have reviewed experimental results performed under subconfluent conditions, in which cell density is kept to a lower value in order to reduce the possible effect of cell–cell interaction. However, to more closely reproduce a tissue structure *in vitro*, in some experiments cells are grown until a confluent configuration is achieved.

A first consequence of these experimental conditions is that, as depicted in Fig. 7(a), it may happen that cells and their stress fibres cannot orient at the same time along the directions θ and $-\theta$, because of cell–cell contact and hindrance (Dartsch et al., 1986; Wang et al., 2018). Thus, a choice between the two equivalent symmetric orientations
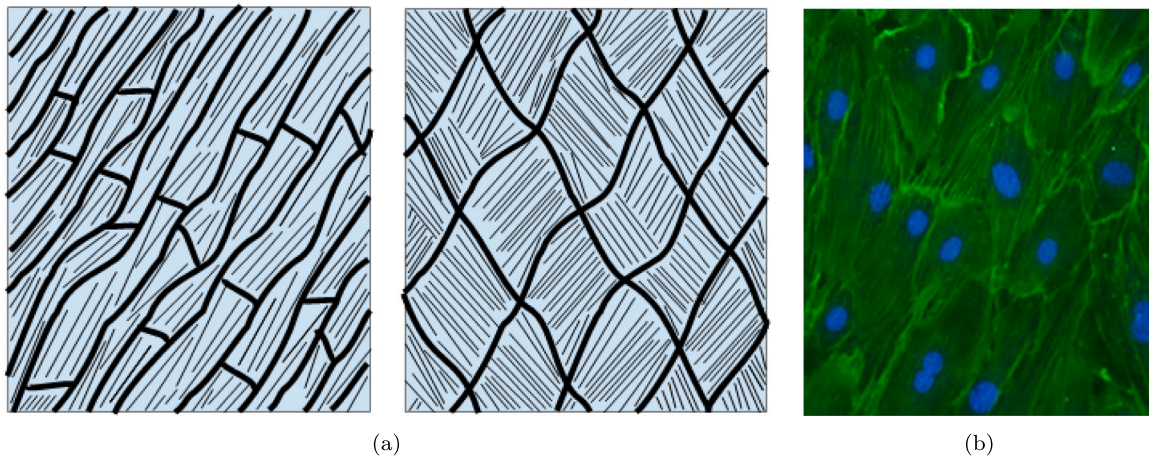
Fig. 7. (a): Sketch of possible stress fibre orientation in confluent cells (redrawn from Takemasa et al. (1998)). (b): Experimental microscopic view of confluent aligned cells, taken with permission from Iwaki et al. (2009). The stretching direction is horizontal.

has to be made, leading to an advantage from a statistical viewpoint. The distribution of orientations shows therefore only one peak in the interval $[0, \pi]$, so that the problems in statistically describing the outcome of the experiments – discussed before – are often eliminated. However, also in the confluent condition, some difficulties in defining the orientation angle may arise. For instance, in the work by Takemasa et al. (1997, 1998), cells acquire a rhomboidal-like shape and so the confluent structure has two symmetric directions, as sketched in the right panel of Fig. 7(a).

We summarise the results about confluent cells in Table 3. As in the sub-confluent case, some authors report an oblique angle (Dartsch et al., 1986; Takemasa et al., 1997; Matsugaki et al., 2013) and others a perpendicular alignment (Sumpio et al., 1988; Kaunas et al., 2006; Yoshigi et al., 2003; Ives et al., 1986). However, it is worth to advise that, also in this case, the word *perpendicular* is sometimes used improperly. For instance, Iwaki et al. (2009) described the arrangement they observed in this manner, but from their images, reported in Fig. 7(b), it rather seems that $\theta_{eq} \approx 60°$ is a more appropriate descriptor of the orientation. Similarly, in the work by Wang et al. (2018) the term "perpendicular" is used to denote an orientation of nearly 75°. Hence, if a precise estimate of the alignment angle is to be obtained, one should be careful since several experimental reports describe any shift towards 90° as perpendicular.

Differently from sub-confluent conditions, the preferential orientation angle is sometimes found to depend on the imposed stretching amplitude. For instance, Takemasa et al. (1997, 1998) span from $\varepsilon_0 = 10\%$ to $\varepsilon_0 = 110\%$, measuring a mean inclination $\bar{\theta} \approx 60°$ up to $\bar{\theta} \approx 69°$. A regression line $\bar{\theta} = 59.807 + 0.081\varepsilon_0$ is fitted in the work by Takemasa et al. (1997), whereas the linear relation between the angle and the amplitude becomes $\bar{\theta} = 59.0 + 0.09\varepsilon_0$ in Takemasa et al. (1998), with ε_0 expressed in percentage.

In both cases, these relations suggest that an increase in amplitude makes the cell to orient more perpendicularly to the strain. For comparison, we advise that the angles reported in both the articles (Takemasa et al., 1997, 1998) are measured with respect to the orthogonal direction of the deformation, while here we prefer to report the angles with respect to the strain direction. In the work by Takemasa et al. (1998), the biaxiality ratio ranges from $r = 0.7$ when $\varepsilon_0 = 10\%$ to $r = 0.32$ when $\varepsilon_0 = 70\%$ which is known to strongly affect the equilibrium orientation. Moreover, in Takemasa et al. (1998) several other factors possibly influencing the preferential angle are ruled out, including the duration of the stretching, the holding time of the deformation, the frequency, the ECM coating of the substrate (fibronectin, collagen, laminin, vitronectin), and the cell type (human ECs and rat SMCs).

A similar dependence is also found by Dartsch et al. (1986) who measured a mean (computed in $[0, \pi]$) of $\bar{\theta} = 61°$ when $\varepsilon_0 = 5\%$ and

of $\bar{\theta} = 76°$ when $\varepsilon_0 = 10\%$, and the angle ranges with highest probability are $[50°, 60°]$ and $[70°, 80°]$, respectively. Instead, an anomalous behaviour concerning the amplitude of applied strain is reported for confluent esophageal cells by Ritchie and coworkers (Ritchie et al., 2009). The authors state that an amplitude of 2% favours parallel alignment of cells, while amplitudes of 5% and 10% induce a perpendicular reorientation.

Very recently, Gérémie and collaborators (Gérémie et al., 2022) studied the reorientation in a confluent monolayer of intestinal cells undergoing a periodic strain, with parameters mimicking the peristaltic movement *in vivo*. They found a preferential perpendicular alignment, with about 20% of cells aligned orthogonally to the main stretching direction.

It is important to remark that confluent configurations bring into play the relevant and non-negligible role played by cell–cell interactions. As a consequence, both the biological phenomena and the mathematical modelling become more complex. In fact, as mentioned above, most models tend to work in a sub-confluent framework so that each cell can react independently and the dynamics is simplified.

Regarding the speed of reorientation, as before it is found to increase with ε_0. However, compared to the sub-confluent case, Jungbauer et al. (2008) report that fibroblasts in confluence take a shorter time to reorient (e.g., 60 min at $f = 1$ Hz compared to the 80 and 120 min of the sub-confluent cells). Actually, for larger frequencies, the characteristic reorientation time τ_c does not reach a plateau, but continues to decrease following a power law as clearly evidenced in Fig. 6(a). This suggests an important effect of cell–cell contact, that may avoid the saturation of molecular mechanisms seen in sub-confluent experiments, at least in the range of frequencies tested. At variance, Ives et al. (1986) state that human umbilical vein endothelial cells in less confluent portions of the membrane aligned more rapidly than the ones in zones with higher cell density.

For the sake of completeness, we have to mention that, differently from all previous experiments, Yamane et al. (2007) observed that more than 90% of cardiomyocytes in confluence aligned preferentially along the stretching direction, forming an angle smaller than 30°. A slight tendency to align parallel to the stretch direction is also reported by Collinsworth et al. (2000).

2.1.4. Main findings for cells on 2D isotropic substrates

To sum up, the main *in vitro* findings concerning the response of cells to mechanical deformations of their isotropic, planar substrate are the following:

• Cells respond to cyclic strain of the substrate by reorienting their stress fibres and bodies towards a preferential orientation. The actin cytoskeletal structure is fundamental for this reorientation process.

Table 4

Summary of the main experiments performed in three-dimensional matrices or gels. For each experiment, in addition to the cell type, we report the tested frequencies, amplitudes and preferential orientation. In particular, we use square brackets to denote a range of values. Moreover, in Reynolds et al. (2020) the strain oscillates between 10% and 20%. Abbreviations: SMCs = smooth muscle cells; (b) = bovine; (h) = human; (r) = rat. We denote by ⊥ a perpendicular orientation and by ∥ an overall parallel orientation, though the precise angle is not specified.

Cells in 3D gels				
Cell type	f (Hz)	ε_0 (%)	θ_{eq} (max)	Refs.
(h) bronchial SMCs	0.5	12	0°	Asano et al. (2018)
(h) foreskin fibroblasts	0	≈ 40	0°	Lee et al. (2008)
(h) dermal fibroblasts	0, 1	10	∥	Gauvin et al. (2011)
(r) cardiac fibroblasts	[0.5, 4]	10	$\begin{cases} 0° \text{ (free)} \\ 90° \text{ for } r=0 \end{cases}$	Chen et al. (2018)
(h) vein myofibroblasts	0.5	10	$\begin{cases} 0° \text{ (core)} \\ 90° \text{ (surface)} \end{cases}$	Foolen et al. (2012)
(h) vein myofibroblasts	1	5	$\begin{cases} \perp \text{ (cyclic)} \\ \parallel \text{ (static)} \end{cases}$	De Jonge et al. (2013)
(h) cardiomyocytes	1	$10 \leftrightarrow 20$	strain aligned	Reynolds et al. (2020)
(h, r) cardiomyocytes	0, 1	5	∥	Tulloch et al. (2011)
(b) aortic SMCs	0, 1	5	∥	Kanda and Matsuda (1994)
(r) bone marrow progenitor cells	0, 1	10	∥	Nieponice et al. (2007)

- The response of the cytoskeleton can be observed within some minutes and precedes the one of the cell body, which may take some hours to be completed.
- The preferential orientation is *perpendicular or oblique* with respect to the main stretching direction. The biaxiality ratio *r*, related to the amount of tension and compression transmitted to the substrate and therefore to the cells, seems to play an important role in the precise quantification of the orientation angle.
- The results concerning the preferential equilibrium angle of cells appear to be *robust* with respect to the frequency and the amplitude of the applied cyclic deformation, as well as with respect to the stiffness of the substrate and its coating. This is true provided that all these mechanical factors are greater than a certain lower threshold, below which no response is triggered. In addition, an increase in frequency and amplitude leads to a more rapid and more pronounced orientation of stress fibres and cells.
- A wide variety of cell types turns out to be mechanically responsive: fibroblasts, endothelial cells, vascular smooth muscle cells, neural-like cells, mesenchymal stem cells, intestinal cells, as evident from Tables 1–3.
- In the confluent case, the effect of cell–cell contact comes into play and may lead to differences in the preferential orientation. Moreover, if experiments are performed under confluence, reorientation is sometimes found to be faster (Jungbauer et al., 2008).

2.2. Cells in three-dimensional matrices

The two-dimensional setting with cells adhering on a planar substrate has several advantages, but in some cases might result in a simplification of the real environment experienced by cells *in vivo*. Therefore, experiments culturing cells in three-dimensional matrices and fibre networks (usually made of collagen or fibrin) or in tissue engineered constructs have been performed by numerous groups. In particular, cells in a three-dimensional ECM are surrounded by fibres, and adhesive sites are active all around them. On the one hand, this leads to the fact that cells tend to elongate together with the ECM, due to the phenomenon of contact guidance. On the other hand, the imposed stretch induces both a topological and a mechanical anisotropy. Indeed, cells embedded in a 3D gel may exert traction forces, compact the surrounding matrix and also alter its anisotropy by realigning the fibres, thanks to the protrusion of pseudopodia (Feng et al., 2014). For instance, collagen gel compaction and contraction by fibroblasts,

with development of tension, was already observed in 1982 by Bellows et al. (1982). Then, more recent experiments demonstrate that cells embedded in a matrix, possibly constrained at its boundaries, and left in static conditions tend to compact the sample and to develop stresses (Chen et al., 2018; Foolen et al., 2012). The interplay between contact guidance cues by collagen fibres and mechanical stimuli coming from periodic deformations becomes therefore more complex. Moreover, very soft gels or matrices do not transmit all the applied stretch to the cells (Chen et al., 2018; Ujihara et al., 2015), and it is more difficult in such cases to precisely quantify the strain sensed by the cells with respect to the externally controlled deformation (De Jonge et al., 2013; Rihel et al., 2012). Indeed, soft gels mimicking the ECM may undergo alterations in their mechanical properties due to the applied stretches and to cell traction forces.

Overall, as reported in Table 4, the result is that cells in 3D structures are more prone to orient along the main stretching direction (Asano et al., 2018; Chen et al., 2018; De Jonge et al., 2013; Foolen et al., 2012; Gauvin et al., 2011; Lee et al., 2008; Nieponice et al., 2007; Reynolds et al., 2020; Ritchie et al., 2009; Tulloch et al., 2011). In this respect, an interesting comparative study between the 2D and 3D cases for vascular smooth muscle cells undergoing periodic deformations was performed by Bono et al. (2016). In accordance with previous works, the experiments confirmed that in two-dimensional monolayers there was a preference for the perpendicular orientation (80–90 degrees), while in three-dimensional collagen gels parallel alignment (0–10 degrees) was predominant.

In static conditions, cells tend to align with the direction of sustained stretch or with the direction of boundary constraints (see Chen et al., 2018; Asano et al., 2018; De Jonge et al., 2013; Gauvin et al., 2011; Kanda and Matsuda, 1994; Lee et al., 2008; Nieponice et al., 2007; Tulloch et al., 2011; Matsumoto et al., 2007; Hu et al., 2009; Wakatsuki and Elson, 2003). Specifically, the role of mechanical constraints in 3D tissue constructs was firstly underscored by Nieponice et al. (2007). Then, the subtle balance between contact guidance, constraints, and stretch avoidance in 3D cultures is vividly highlighted by Foolen et al. (2012), who performed extensive experimental analyses on myofibroblasts cultured in collagen/matrigel gels. In detail, if cells were left free to compact the gel for a few days with deformation restrained in one direction, an orientation towards the direction of the applied constraint was observable. Instead, if the gel deformation was constrained in two perpendicular directions, the cells did not show a preferential alignment and oriented in both the constrained

directions equally. When cyclic stretch was applied after static culture, to study the combined effect, the results unveiled interesting differences across the gel depth. Cells in the core of the specimen exhibited alignment along the main strain direction, while those at the top and bottom surfaces of the gel strongly aligned perpendicularly, as in planar membranes. In fact, in the core, the effect of collagen fibres is sterically restrictive, while on the boundary the strain-avoiding mechanism overwhelms the anisotropy induced by ECM fibres. Indeed, if collagen density within the core is reduced, reorientation towards the perpendicular direction is observed throughout the whole tissue sample (Foolen et al., 2012). Later, the same group (Foolen et al., 2014) showed that, even at high collagen densities, activation of protein Rho may result in SFs reorientation away from stretch, as already put in evidence for 2D settings (Kaunas et al., 2005; Lee et al., 2010). Overall, the interplay between matrix density, deformation, and Rho signalling pathway appears therefore important in 3D cell alignment.

Other studies that highlight variations of collagen and cell alignment throughout the depth of 3D tissue constructs are those by Boerboom et al. (2008) and by Rubbens et al. (2009). In both of them, when samples were intermittently strained, collagen fibres and cells were found to align perpendicularly or obliquely to the stretch direction at the surface, whereas parallel alignment to the deformation emerged deeper into the 3D matrix.

Chen et al. (2018) found slightly different results from Foolen et al. (2012). More in detail, they firstly pre-cultured the cells for 24 h in a 3D gel with deformation restrained in two directions. After that, the gel was subjected to a uniaxial cyclic elongation at 0.5 Hz, and parallel alignment to the strain was achieved. Instead, if the specimen underwent pure uniaxial stretching (with $\varepsilon_{yy} = r = 0$) no alignment was observed. Unlike Foolen et al. (2012), no difference was evident in orientations between the surface and the core of the gel.

Additional relevant results about the mechanical stimulation of 3D matrices are due to Lee et al. (2008), who stretched a fibroblast-populated 3D collagen gel firstly in one direction for a time t^*, with $t^* \in \{5, 24, 48, 72\}$ hours, and then in the orthogonal direction. It was observed that, when the stretching direction is switched, the cells reorient themselves towards the direction of the newly applied load. The time required for reorientation was longer in specimen with larger values of pre-stretching time t^*, indicating that the remodelling of strongly aligned tissue constructs may be slower.

Parallel alignment of cells to strain in 3D was also found by Gauvin et al. (2011), Wakatsuki and Elson (2003), and Asano et al. (2018), both for step deformations and for cyclic stretching. Moreover, in Gauvin et al. (2011) and Wakatsuki and Elson (2003), it was highlighted that the application of a mechanical stimulus induced changes in the mechanical properties of the tissue engineered samples, with increased anisotropy and stiffness along the preferential direction. This is due do the compaction of the collagen gel by the cells, which can exert pulling forces up to 8 mN (Wakatsuki and Elson, 2003). External mechanical fields can therefore be useful to modulate the mechanical properties in the design of engineered tissues.

In addition to gels, cellular alignment is also analysed in artificial tissue samples, like scaffolds and grafts. For instance, to reproduce the heart environment as realistically as possible, Tulloch et al. (2011) assembled engineered 3D constructs of cardiomyocytes and collagen, both for rodent and human cells. The artificial grafts were then analysed from a mechanical viewpoint. In all cases, static and cyclic stretch promoted alignment parallel to the stress with no significant differences between the two loading conditions. However, the authors themselves warn that spontaneous contractions are observed in cells for both situations, and this may influence the results.

In contrast with almost all the experiments on three-dimensional matrices, Cha et al. (2006) found that smooth muscle cells in a 3D porous scaffold oriented perpendicularly to the cyclic stretching direction; however, even if cells were firstly seeded onto the surface of the polymeric matrix, they observed a consistent number of stretched

cells to penetrate deeper in the scaffold, which makes it difficult to discriminate the effects of contact guidance and cyclic strain.

To summarise, for cell alignment in three-dimensional assays we have the following relevant features:

- Cell alignment in 3D fibrous matrices with high collagen/fibre densities is not primarily guided by stretch avoidance, as for planar substrates undergoing cyclic strain. Contact guidance due to collagen fibres, which may also be remodelled by cells, competes with cyclic strain avoidance.
- An orientation of the cells parallel to the deformation is frequently observed, especially in the core of the samples. Instead, at the surface, where contact guidance is less effective, the cells align perpendicularly or obliquely as in 2D substrates.
- If soft matrices are used, like those composed of collagen, compaction of the tissue sample by the cells due to boundary constraints as well as cellular contractility (Reynolds et al., 2020) are suggested to be important in determining cell alignment.
- The interplay of all these factors is not trivial, even if the 3D situation is the one which most faithfully represents the *in vivo* conditions.

## 3. Review of mathematical models

The consistent amount of experimental data reviewed in Section 2 shed some light on the cell response to mechanical stimulations. However, there are still many unanswered questions, and the precise biological and physical mechanisms that underlie cellular reorientation are not fully clear. In this respect, starting from the early 2000s, mathematical models were proposed in order to provide a better understanding of experimental findings.

Several approaches have been adopted so far to target the modelling of cellular reorientation but a sharp classification is difficult to perform, since several models deal with multiple tools and often with multiple scales. Here, we aim at providing a categorisation by highlighting the main modelling structures and instruments upon which the models are grounded. Specifically, in Section 3.1 we present models that treat the stress fibres as active structures able to contract. Then, in Sections 3.2 and 3.3 we respectively discuss the strain and stress avoidance approaches. In the framework of Continuum Mechanics, Section 3.4 reviews some very relevant results about the use of elastic energies to find the cell preferred orientation. Then, Section 3.5 reviews the approaches that take viscoelasticity into account, whereas Section 3.6 introduces some models that employ a tensegrity description of the cell. Finally, Section 3.7 provides an overview of articles in the Statistical Mechanics and optimal control framework. Such a subdivision is not meant to be mutually exclusive, and some works will be discussed in more than one Section.

3.1. Modelling stress fibres as active contractile structures

Most of the experimental works agree upon the importance of the highly mechanosensitive structure of actin stress fibres, which appear to have a fundamental role in cell reorientation. These fibres are able to develop contractile forces thanks to the bundling of actin filaments and myosin heads: such a structure somehow reminds of the one of sarcomeres, i.e. the elementary contractile units composing muscles, as in Fig. 8. Even though there are several differences between SFs and sarcomeres (Kaunas et al., 2011), the similarities motivated some studies to tackle the problem of cell and cytoskeletal realignment by using an active contractility approach for SF filaments.

In this respect, a starting point for several modelling attempts of cell stress fibres orientation is the framework proposed by Deshpande and collaborators (Deshpande et al., 2006, 2007). In a series of papers, the authors developed a model for cell cytoskeletal contraction as an active phenomenon following an external chemical stimulus. The stress fibres
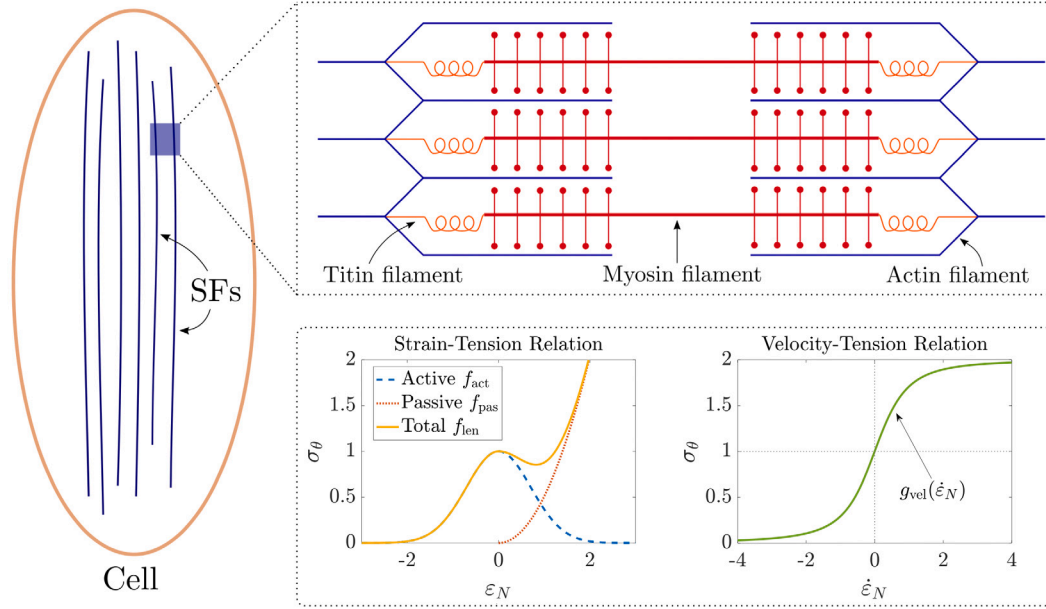
Fig. 8. Top panel: Sarcomeric-like structure of cellular stress fibres for modelling purposes, discussed in Section 3.1. The fibres are considered as composed by sequences of active contractile structures: the reciprocal sliding of actin and myosin filaments, as well as the elasticity of titin filaments, determine the development of internal tension. Bottom panel: strain–tension relation and velocity–tension relation used in some models (Vernerey and Farsad, 2011; Obbink-Huizer et al., 2014). The velocity–tension curve is derived from the classical Hill dynamics for muscles. Instead, the strain–tension total response function (yellow curve) is the sum of an active (dashed blue curve) and a passive (dashed red curve) component. In particular, an increase in the SF strain ε_N provokes an increase in the passive stress, whereas the active contraction of the fibre is maximum when there is no strain, i.e., $\varepsilon_N = 0$. Both ε_N and $\dot{\varepsilon}_N$ are normalised with respect to a reference value (Vernerey and Farsad, 2011).

are considered as active filaments capable of developing an internal tension, which resembles a classical Hill-like model for cross-bridge dynamics in muscles (Hill, 1938). Moreover, the activation level of the fibres $\eta \in [0, 1]$ oriented at an angle θ is another key variable of their model that evolves according to an equation like

$$\frac{d\eta}{dt}(t; \theta) = k_+(1 - \eta)C - k_- \eta \, \hat{\sigma}(\eta, \theta). \tag{5}$$

The first term on the right-hand side accounts for SF activation with a rate k_+, promoted by the concentration of a chemical signal C and proportional to the amount of inactive fibres $1 - \eta$. Instead, the second term describes stress-related SF dissociation, in which $\hat{\sigma}$ embeds the active SF tension following a Hill model. In particular, in Deshpande et al. (2006, 2007), such tension is assumed to stabilise fibres and therefore to reduce their dissociation rate, with $\hat{\sigma} \to 0$ as tension increases. The first versions of this model were able to reproduce a number of interesting experimental features about the cytoskeletal active contraction, such as a decrease of the force exerted by the SFs on softer substrates and the concentration of SFs activation near sites of localised tension. A successive work by Wei et al. (2008) introduced the cyclic deformation and studied the subsequent remodelling of the cytoskeleton. Results in the periodic case capture the perpendicular preferential orientation if a pure uniaxial stretch ($r = 0$) is applied to the substrate, which is in line with several experimental settings described in Section 2.1. Furthermore, the degree of alignment is found to increase with the maximum amplitude of the oscillation ε_0 and with the frequency ω. Instead, in the simple elongation or biaxial cases (see Fig. 2), two symmetric preferential orientations are found, which are given by the directions where the strain rate is null, namely,

$$\theta_a = \pm \arctan\left(\frac{1}{\sqrt{r}}\right). \tag{6}$$

However, as we will discuss in Section 3.2, such a prediction coincides with the one obtained with the strain avoidance approach, suggesting that the cell aligns along the direction of minimal stretch. An interesting prediction found in Wei et al. (2008) is that changes in the stress

fibre sensitivity to external stimuli may enhance their alignment as effectively as an increase in the stretch magnitude, coherently with some experimental findings (Kaunas et al., 2005).

A different framework, though still based on SFs activation and cross-bridge contraction dynamics, is developed by Vernerey and Farsad (2011). The authors propose a constrained mixture model, accounting for both passive elasticity and active contraction of the fibres that is driven by length–tension and velocity–tension relations, shown in Fig. 8. Specifically, the stress fibre density ϕ_θ in direction θ is assumed to be governed by an equation in the following form:

$$\frac{\partial \phi_\theta}{\partial t} = k_+ \phi_m - k_- \phi_\theta + k_s \sigma_\theta \phi_m, \tag{7}$$

neglecting advection. Eq. (7) describes the assembly of SF with a rate k_+ proportional to the concentration of monomeric actin ϕ_m and SF dissociation with a constant rate k_-. In addition, the last term on the right-hand side accounts for stress-induced SF formation, with σ_θ being the normalised tension in the fibres defined by

$$\sigma_\theta = f_{\text{len}}(\varepsilon_N) g_{\text{vel}}(\dot{\varepsilon}_N) = [f_{\text{act}}(\varepsilon_N) + f_{\text{pas}}(\varepsilon_N)] g_{\text{vel}}(\dot{\varepsilon}_N) \tag{8}$$

with the functions $f_{\text{len}}(\varepsilon_N)$ and $g_{\text{vel}}(\dot{\varepsilon}_N)$ represented in the bottom panel of Fig. 8 (yellow and green curves) with respect to the strain ε_N and the strain rate $\dot{\varepsilon}_N$ along the direction of the SF, respectively. More specifically, f_{len} models the SF response to length changes and features an active contractility contribution f_{act} (dashed blue curve in Fig. 8) and a passive one f_{pas} (dashed red curve in Fig. 8). Instead, $g_{\text{vel}}(\dot{\varepsilon}_N)$ represents the tension-velocity Hill-like relation, shown in Fig. 8 by a green curve. A direct comparison with Eq. (5) allows to observe that, differently from Deshpande et al. (2006) where it was assumed that stress reduced SF dissociation, in Vernerey and Farsad (2011) the same stress promotes SF formation. The model provides interesting predictions and insights into cell contractility mechanisms but, as pointed out in Obbink-Huizer et al. (2014), it is not completely accurate in the description of reorientation, since it would predict that a large amount of fibres is aligned to the strain direction. A similar constrained mixture approach had been used previously by Na et al.

(2007) who developed a theoretical tool to describe the nonlinear elasticity of actin in equi-biaxial mechanical tests.

Later, in Obbink-Huizer et al. (2014), the advantages of the models by Deshpande et al. (2006) and Vernerey and Farsad (2011) are combined, in an attempt to overcome the limitations of both. In particular, an evolution equation for the stress fibre density $\Phi(t; \theta)$ in direction θ akin to Eq. (7) is proposed. However, the passive response of SF is dropped and only the active contraction function f_{act} is assumed to influence the formation of new fibres.

Then, this type of models was further developed by Vigliotti et al. (2016) who proposed a very sophisticated thermodynamical framework, coupling the macroscopic evolution of the cytoskeleton with microscopic considerations about stress fibre formation. The model is capable of accurately predicting several experimental features, such as the discrepancy between perpendicular alignment on 2D substrates and parallel alignment to the deformation in 3D gels, as discussed in Section 2.2. Nevertheless, the dependence on the biaxiality ratio r is not described in this framework. Further investigations adapted the previous model to simulate the reorientation of cells on grooved substrates (Vigliotti et al., 2015; Ristori et al., 2016), the generation of transient force (McEvoy et al., 2019) experimentally noticed (Wille et al., 2006), and the alignment in 3D collagen gel constructs (Chen et al., 2018; Reynolds et al., 2020) described in Section 2.2.

The approach pursued by Hsu and coworkers (Hsu et al., 2009, 2010; Kaunas and Hsu, 2009) is slightly different and consists in a purely kinematic description of SF disassembly and preferential realignment, based on experimental reports that fibres are pre-stretched at a homeostatic level (Lu et al., 2008). Mechanical perturbations then destabilise this state and provoke a reorganisation of the cytoskeleton. A first version of their model was based on a deterministic evolution equation for the fibres, with a time rate depending on the deviation from their homeostatic pre-stretch (Kaunas and Hsu, 2009). In subsequent works, the dynamic turnover of SFs was then described by a stochastic formulation (Hsu et al., 2009, 2010), with the probability of stress fibre disassembling during the time interval Δt which is taken to be

$$P = \left[k_0 + k_1 \left(\frac{\lambda^i - \lambda_0}{\lambda_0} \right)^2 \right] \Delta t,$$

where λ_0 is the fibre homeostatic pre-stretch that is experimentally found to be $\lambda_0 \approx 1.1$ (Lu et al., 2008) and λ^i is the current fibre stretch. If a SF is disassembled, a new SF oriented randomly with a stretch λ_0 is immediately built. The model turns out to be effective in predicting the reorientation away from the stretching direction and the absence of alignment for equi-biaxial deformation. However, the model seems to suggest that cells align along the direction of minimum deformation, which is not always accurate as we will discuss in Sections 3.2–3.4. Moreover, another difference between Hsu et al. (2010) and Deshpande et al. (2006) lies in the choice of initial conditions. While in the former SFs are considered as randomly distributed at the beginning, the latter takes a cell devoid of fibres at the initial time instant and studies its rebuilding.

The same group (Kaunas et al., 2011; Tondon et al., 2012) successively proposed a sarcomeric model of a SF as a passive elastic element coupled with an active contractile myosin filament, borrowing again ideas from muscle contraction. The results are able to capture the different evolution of SF orientation due to high and low frequency periodic strains. In particular, high frequencies induce changes in SF length which are faster than the myosin can respond, whereas low frequencies allow the SF to maintain a constant force by myosin sliding. An increase in the frequency also decreases the circular variance, as shown in Fig. 9.

Analogous ideas are found in the work by Chen et al. (2012), where the role of focal adhesions is taken explicitly into account in the elasto-sarcomere picture of SF. The existence of two activation modes for the SF, called *localised* and *homogeneous* activation, introduces two intrinsic

time scales. These are related to a lower and an upper frequency, respectively, which represent the minimal and maximal threshold frequencies observed experimentally (Jungbauer et al., 2008). Again, the model predicts that SFs reorient towards the direction of least substrate deformation.

Another interesting contribution to the structural modelling of SFs is the one by Qian and coworkers (Qian et al., 2013; Lin et al., 2020), who presented a mechano-chemical theory at the microscale that accounts for the formation of ligand–receptor bonds between cell and substrate through simple first-order kinetics. The authors report several intriguing predictions, such as differences between reorientation on stiff and soft substrates, amplitude and frequency thresholds, and the role of the protein Rho (Qian et al., 2013). However, a consistent limitation of this model regards the fundamental hypothesis that cells align along the direction of maximum actin density, which is not strongly corroborated by experiments and does not clarify why the cell should prefer any direction. A refinement is then introduced by the same authors in Lin et al. (2020) for neuron reorientation, accounting also for changes in neuronal length.

Finally, we mention the works by Kong et al. (2008) and Zhong et al. (2011), in which a multiscale link between the focal adhesion bond microscopic dynamics, the turnover of stress fibres and the cell–matrix coupling is drawn.

3.2. Strain avoidance

Historically, the very first modelling approaches to describe cell reorientation under stretch were based on a strain minimisation principle, which led to naming the phenomenon as *strain avoidance* (Buck, 1980; Wang et al., 1995). According to this hypothesis, the cell would preferentially align along the directions where it feels the minimum possible strain, so as to minimise the discomfort and the cyclic elongations of its cytoskeleton. Through standard calculations, we can therefore write the strain experienced along a direction $\mathbf{N} = (\cos \theta, \sin \theta, 0)$ as

$$\varepsilon_N = \varepsilon_{xx} \cos^2 \theta + \varepsilon_{yy} \sin^2 \theta = \varepsilon_{xx}[(1 + r) \cos^2 \theta - r], \qquad (9)$$

where $\varepsilon_{xx}, \varepsilon_{yy}$ are the principal strains and $r := -\varepsilon_{yy}/\varepsilon_{xx}$. A direct application of the minimal strain principle to Eq. (9) readily allows to state that the preferred directions are given by

$$\theta_{eq} = \arccos \sqrt{\frac{r}{1 + r}} = \arctan \sqrt{\frac{1}{r}}, \qquad (10)$$

which is equivalent to Eq. (6). In particular, for $r = 0$, the only preferential orientation is $\theta_{eq} = \frac{\pi}{2}$. As shown in Fig. 10, θ_{eq} corresponds to the intersection of the strain curve, defined by Eq. (9), with the zero strain line.

With respect to this approach, Takemasa et al. (1998) were among the first to suggest that the stress fibre orients to minimise changes in its length during cyclic stretch, i.e. along the direction of null stretch, based on geometrical considerations. Then, Wang et al. (1995) proposed a more refined description based on strain avoidance, under the following assumptions:

(i) cell reorientation is initiated by the strain along the cell major axis;

(ii) each cell has an axial strain threshold it can sustain, and such threshold is normally distributed in the cell population, with 3% mean and 1.5% standard deviation estimated for melanocytes;

(iii) the cell avoids any direction where the axial strain exceeds its threshold;

(iv) the final orientation is selected randomly among the directions where the axial strain is less than the threshold.

Although some of the previous assumptions are quite strong, this is one of the first attempts to rationalise the strain avoidance mechanism, already observed in experiments by Buck (1980) and Dartsch and Hammerle (1986), Dartsch et al. (1986). The model by Wang and
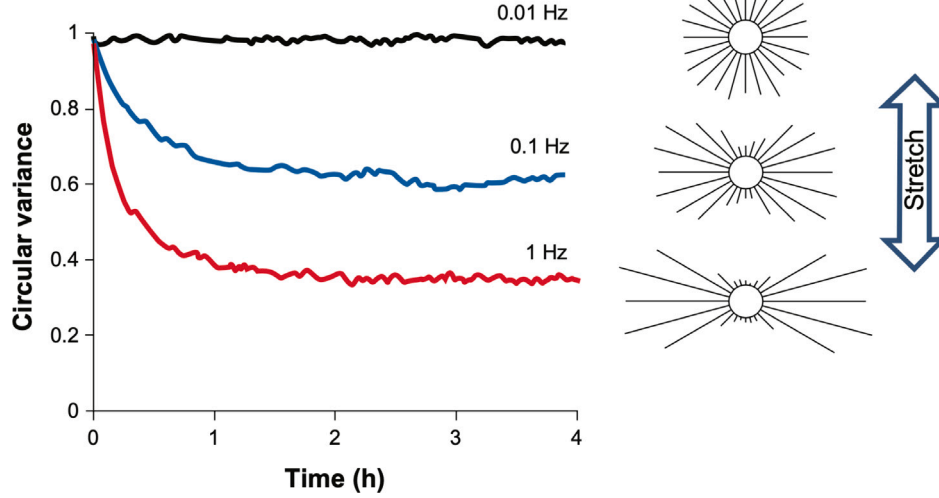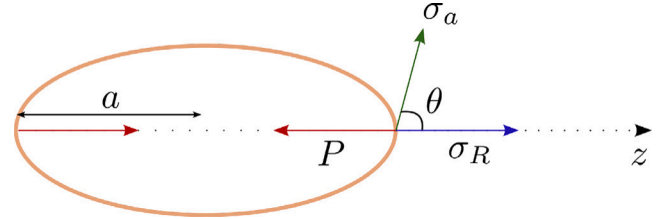
Fig. 9. Evolution of circular variance in time for different applied frequencies, where a model for active contractile stress fibres is proposed. An increase in the frequency leads to a decrease in the circular variance, that is, to a more pronounced orientation of SFs along the orthogonal direction, as shown by the circular histograms.
Source: Taken from Kaunas et al. (2011).
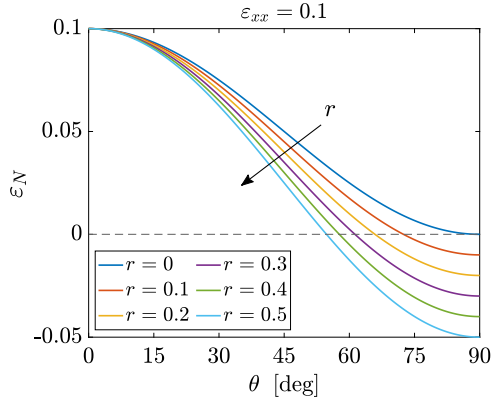
Fig. 10. Axial strain in direction θ, defined by Eq. (9), as a function of the angle for different values of r and a fixed value of $\varepsilon_{xx} = 0.1$. According to the strain avoidance approach, the cell preferential angle defined by Eq. (10) corresponds to the intersection between the coloured curves and the dashed line, which represents zero strain.

Fig. 11. Sketch of the force-dipole model for cell reorientation used in De et al. (2008) and De and Safran (2008). The cell is assumed to have its major axis aligned with the z axis, whereas the externally applied stress σ_a is acting at an angle θ with respect to the cell axis. P is the cell dipole magnitude and σ_R is the subsequent reaction stress developed in the matrix due to active contractility.

collaborators was also used by Barron et al. (2007), who estimated a mean of 1.8% and a standard deviation of 0.75% for the normal distribution of tolerable strain in a population of endothelial cells. Neidlinger-Wilke and coworkers (Neidlinger-Wilke et al., 2001) estimated instead an axial strain limit of 6.4% for osteoblasts and of 4.2% for fibroblasts. More recently, a very similar approach was followed in the work by Morioka et al. (2011), where a simple linear elastic model for SFs and MTs is proposed, though the role of the latter is not clear experimentally (see Section 2.1).

A refinement of previous descriptions of actin filament dynamics was provided by Wang in 2000 (Wang et al., 2000). In particular, he evaluated the change in the strain energy of a fibre due to the action of the axial strain ε_f transmitted to it. The model is then developed under the hypothesis that, in absence of deformation, each filament of actin owns a basal strain energy E_b, related to the pre-strain of the SF due to its inherent tension. The total energy of the deformed fibre E_f is then calculated by assuming that the SF behaves as a linear elastic filament with an applied elongation ε_f. Disassembly of SFs is assumed to occur if the strain energy E_f is decreased to zero or increased to twice the basal energy E_b. This assumption allows to identify through Eq. (9) an

interval of orientations:

$$\theta \in \left[\arccos \sqrt{\frac{r}{1+r} + \frac{B}{(1+r)\varepsilon_{xx}}}, \; \arccos \sqrt{\frac{r}{1+r} - \frac{B}{(1+r)\varepsilon_{xx}}} \right], \quad (11)$$

where B is a parameter related to the amount of fibre pre-strain and initial length before deformation. It is immediate to observe that in the limit $B \to 0$, which corresponds to a vanishing pre-strain of SFs, the above interval collapses to the angle defined by Eq. (10), that is again the direction of null strain. In addition, increasing the applied strain ε_{xx} (without conflicting with the small deformation assumption) leads as well to a narrowing of the range of preferential angles. This correlates with the fact that higher strain amplitudes are associated with a smaller range of observed orientation angles in experiments, and therefore to more peaked probability distributions as shown in Fig. 4.

A different but somehow related approach is pursued by De and co-workers (De et al., 2008; De and Safran, 2008). Using a coarse-grained picture, they model the cell as an anisotropic force dipole (Schwarz and Safran, 2002; Bischofs and Schwarz, 2003) as sketched in Fig. 11, to mimic the action of a stress fibre along a given direction. In their work, the focus is on how the cell readjusts its contractile activity by developing a force along its major axis, which can be reoriented as a consequence of perceived mechanical cues. Additionally, the authors assume that such a reorganisation is driven by the maintenance of an optimal level of strain, which is achieved by the minimisation of a proper energy function $\mathcal{U}(P, \theta)$, with P being the contractile dipole force and θ the angle of orientation with respect to the applied stress (see Fig. 11). Specifically, the following system of equations is proposed
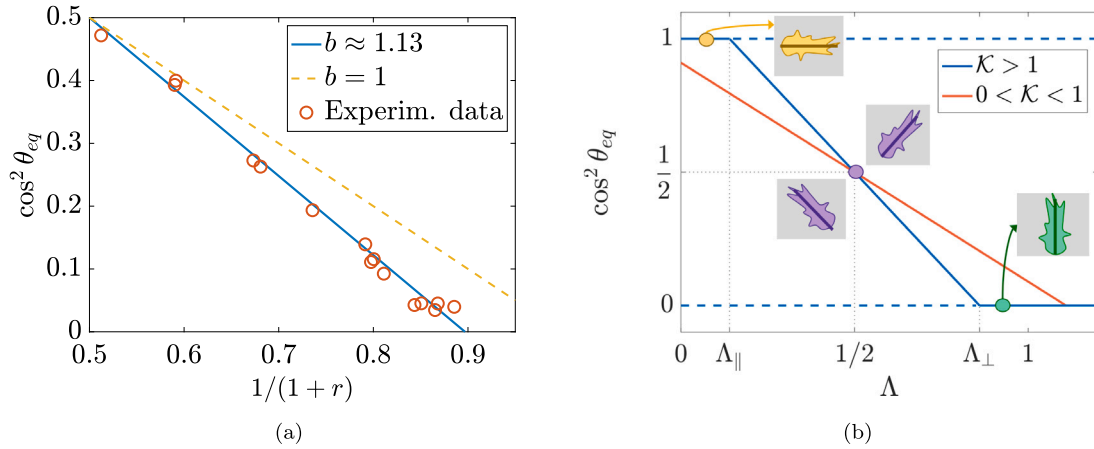
Fig. 12. (a): Relation between the orientation angle θ_{eq} and the parameter r, according to the model in Eq. (16) proposed by Livne et al. (2014). The line with slope $b \approx 1.13$ accurately fits the experimental data, whereas the strain avoidance approach, corresponding to $b = 1$, does not (data taken from Livne et al., 2014). (b): Bifurcation diagram found in Lucci and Preziosi (2021) for $\mathcal{K} > 0$.

in De et al. (2008):

$$\tau_P \frac{dP}{dt} = -\frac{\partial \mathcal{U}}{\partial P}, \qquad \tau_\theta \frac{d\theta}{dt} = -\frac{\partial \mathcal{U}}{\partial \theta}. \tag{12}$$

The steady state solutions for the angle are found to be $\theta_{eq} = 0$, $\theta_{eq} = \pi/2$, and a third oblique one which, if the interaction forces with the matrix are negligible, is given by

$$\cos^2 \theta_{eq} = \frac{r}{1+r}, \tag{13}$$

which again corresponds to the minimal strain direction. As we will discuss in Section 3.3, in De et al. (2008) the possibility that cell remodelling aims at maintaining a target stress rather than a target strain is also investigated.

We conclude this Section by mentioning that a similar approach may be generalised to the case of more than one cell (Zemel et al., 2006). In addition, more recent works, still employing the anisotropic cell dipole description, have been focused on the role of focal adhesions (De, 2018) and on their catch-bond dynamics (Kong et al., 2009). Finally, in the work by Safran and De (2009) and Faust et al. (2011) a random noise is added when studying the reorientation of cell dipoles.

3.3. Stress avoidance

As just mentioned, in the work by De and Zemel (2007), De et al. (2008) and De and Safran (2008) the alternative hypothesis about the existence of a target stress is examined, within a framework akin to the one discussed in the previous Subsection. Specifically, if a single cell acting like a force dipole is considered, it is assumed that its contractile activity is devoted to maintaining an optimal local stress. Such a goal is performed by minimising a proper energy function of the cell, that tends to drive the stress it perceives towards the target value. In this case, neglecting the influence of the extracellular matrix, the only orientations that minimise the energy are $\theta_{eq} = 0$ and $\theta_{eq} = \pi/2$. The latter is the stable one and corresponds to the direction of minimal stress, if a uniaxial applied stress is considered. Therefore, the stress avoidance approach seems to predict that the preferential orientation is always perpendicular to the deformation. To obtain oblique orientations, it appears to be necessary to include the interaction energy with the ECM. The authors then study the response of such a dipole model to both static and cyclic stresses (De et al., 2008; De and Safran, 2008). For the former, results predict an alignment parallel to the stress, while the latter induce a perpendicular or oblique orientation. Moreover, for very low frequencies, their theory suggests that cells align nearly parallel to the applied load. The dependence of the reorientation time on the frequency is also considered, in accordance with experimental results (De and Safran, 2008).

3.4. Elastic energy approaches

In order to disentangle the dichotomy between optimal strain and optimal stress, Livne and coworkers (Livne et al., 2014) performed an extensive series of experiments carefully controlling the biaxiality ratio $r \in [0, 1]$. In this way, the authors were able to show that neither the zero strain direction given by Eq. (6) nor the zero stress directions were accurate in fitting their experimental data. Specifically, for low values of r, a deviation from the zero strain prediction up to 10° emerged, which was 20 times greater than the error bars. In the zero stress case, such a discrepancy was even worse (Livne et al., 2014). Therefore, they suggested a novel approach, based on a different standpoint: instead of looking for the zero strain direction, the cell reorients to target the minimum of the passively stored 2D elastic energy. In other words, the cell attempts to minimise the energy expenditure and not the stress or strain, which is different from previous perspectives. Working in the framework of linear elasticity, they write the energy as a function of the orientation angle θ as

$$\mathcal{U}_{\text{cell}} = \frac{1}{2} K \varepsilon_{xx}^2 \left[\frac{(1+r)\cos^2 \theta - 1}{b} + (1-r) \right]^2 + f(r), \tag{14}$$

with $f(r)$ a function independent of θ, while K and b are material parameters. Then, they consider a dissipative evolution dynamics for the angle in the form

$$\gamma \frac{d\theta}{dt} = -\frac{d\mathcal{U}_{\text{cell}}}{dt}, \tag{15}$$

with γ representing the resistance of cells to reorientation. The stationary points of the energy are calculated for an applied periodic strain $\varepsilon_{xx}(t) = \frac{1}{2} \varepsilon_0 (1 - \cos \omega t)$ averaged over a period, since the frequency is considered to be high. In particular, three steady states for cell orientation are found: $\theta_{eq} = 0$, i.e. parallel orientation, $\theta_{eq} = \pi/2$, i.e. perpendicular alignment, and a third oblique one which satisfies

$$\cos^2 \theta_{eq} = \frac{b(r-1) + 1}{1+r} = b + \frac{1-2b}{1+r}. \tag{16}$$

It is worth to stress that Eq. (16) provides a linear relation between $\cos^2 \theta_{eq}$ and $1/(1+r)$ for the oblique angle, and a fitting of data gives a value of the parameter $b \approx 1.13$. Such a prediction appears to be in excellent agreement with their experimental data, as shown in Fig. 12, both for the oblique angles as functions of r and for the dynamical evolution of θ, even for amplitudes ε_0 up to 24%. We also remark that the energetic approach pursued in Livne et al. (2014) is different from the one used for instance in De et al. (2008). Indeed, the latter predicted that the oblique angle satisfies Eq. (13), which is equivalent to adopting

a strain avoidance approach and does not coincide with the angle given by Eq. (16), in general.

More recently, in the work by Lucci and Preziosi (2021), the work by Livne et al. (2014) has been generalised to nonlinear elastic energies, to evaluate the impact of high stretches. In particular, a wide class of energies was considered, such as

$$\hat{U} = \frac{1}{2}\mathbf{I} \cdot \mathbb{K}\mathbf{I}, \tag{17}$$

where $\mathbb{K}$ is a symmetric matrix of elastic coefficients and $\mathbf{I} := \left(I_4 - 1, I_5 - 1, I_6 - 1, I_7 - 1, I_8\right)$ the vector of anisotropic invariants, e.g., $I_4 = (\lambda_x^2 - \lambda_y^2)\cos^2\theta + \lambda_y^2$ where λ_x, λ_y are the stretches along the x and y directions, respectively. It was shown that the equilibrium orientations for the cells are found to be $\theta_{eq} = 0, \pi/2$, and an oblique one given by

$$\cos^2\theta_{eq} = \frac{1}{2} + \mathcal{K}\left(\frac{1}{2} - \Lambda\right), \tag{18}$$

where

$$\Lambda := \frac{\lambda_x^2 - 1}{\lambda_x^2 - \lambda_y^2} \tag{19}$$

is a parameter which evaluates the deformation, while $\mathcal{K}$ is a material parameter. As a consequence, a linear relation, similar to Eq. (16) found in the work by Livne et al. (2014), between $\cos^2\theta$ and a proper measure of stretch still holds for a very general elastic energy, even for deformations which do not fall into the linear elastic regime. In this respect, it is worth to notice that, in the linear elastic limit, $\Lambda \approx \frac{1}{1+r}$, recovering an equation analogous to Eq. (16). Moreover, in the work by Lucci and Preziosi (2021), bifurcations were studied, obtaining diagrams like those reported in Fig. 12b. In particular, it is shown that, in the case $\mathcal{K} > 1$ (which seems to be the one obtained by Livne and collaborators (Livne et al., 2014)) there exist two supercritical bifurcations point given by $\Lambda_\parallel := \frac{1}{2}(1 - \frac{1}{\mathcal{K}})$ and $\Lambda_\perp := \frac{1}{2}(1 + \frac{1}{\mathcal{K}})$. As Λ is varied, different stability characters for the three possible orientations (parallel, oblique, perpendicular) are found.

Abeyaratne et al. (2022) employ a similar model for the energy of the stress fibres and also take into account the energy associated with focal adhesions. The latter is modelled as a wiggly energy with many local minima, each one corresponding to a stable configuration for the focal adhesion, to represent the attachment–detachment dynamics. Moreover, these minima are separated by small differences in the angle, since the FAs do not move far before reattaching, and only a small amount of energy is needed to jump from a minimum to the one nearby. The total energy is then obtained by summing the energy of SFs and FAs and adopting an effective kinetic law derived by homogenisation. More specifically, the evolution of the angle is driven by an equation of the form

$$\tau_\theta \frac{d\theta}{dt} = -\frac{\partial \mathcal{U}_{\text{tot}}}{\partial \theta} = -\frac{\partial}{\partial \theta}[\mathcal{U}(\theta; \lambda_1, \lambda_2) + \mathcal{U}_w(\theta)], \tag{20}$$

where τ_θ is a characteristic time. In particular, the total energy $\mathcal{U}_{\text{tot}}$ contains the energy of the SF $\mathcal{U}(\theta; \lambda_1, \lambda_2)$, dependent on the stretches λ_1 and λ_2, and a wiggly perturbation $\mathcal{U}_w(\theta)$, which represents the many possible stable states of focal adhesions. Results show that the influence of FAs might lead the system to get stuck in three ranges of equilibrium angles.

Another elastic energy approach is adopted in the work by Ciambella et al. (2022), where a model for the time evolution of cytoskeletal alignment is proposed within the framework of Continuum Mechanics with remodelling. Specifically, such a model is able to describe the evolution under a periodic strain of two different families of stress fibres, which can realign according to different dynamics and can be properly coupled at the same time. The evolution equations for the two SF types can be summarised as

$$m_p \frac{d\theta_p}{dt} = F_p + F_{ps}, \qquad m_s \frac{d\theta_s}{dt} = F_s + F_{sp}, \tag{21}$$

where θ_p, θ_s are the orientation angles of the different fibres whereas F_p, F_s represent the elastic forces acting on each fibre family and

F_{ps}, F_{sp} provide the coupling forces between the two fibres. By means of a proper constraint, the model is able to recover the results derived in the work by Livne et al. (2014) and Lucci and Preziosi (2021), i.e. Eqs. (16)–(18), as a particular case. Moreover, when two distinct types of SFs are considered, a very good agreement of Eq. (21) with the experimental findings by Roshanzadeh et al. (2020) is found, as shown in Fig. 13.

Then, in a recent work, Gérémie et al. (2022) derived an equation for the equilibrium orientations akin to Eq. (16) starting from a *vertex model*. They define the total mechanical energy as

$$\mathcal{U}_{\text{tot}} = \sum_{i=1}^{N} K_A(A_i - A_0)^2 + \gamma_P P_i + K_P P_i^2, \tag{22}$$

where A_i is the area of the ith cell and P_i denotes its perimeter. Hence, a penalisation on area deformation from the optimal value A_0 is introduced, as well as an energy cost associated with cell perimeter changes and tension. Using a mean-field argument and an averaging procedure, the authors showed that the time-averaged energy for a single cell reads

$$\langle \mathcal{U}_{\text{cell}} \rangle = \kappa \left[(1+r)\cos^2\theta + b(1-r) - 1\right]^2,$$

which leads exactly to Eq. (16). Interestingly, however, the authors in this case found a different fitting value for the parameter $b \approx 2.25$ compared with the one by Livne, probably due to the confluent conditions employed in their experiments.

Other works that have been proposed within an energetic continuum framework are the ones by Lazopoulos and coworkers (Lazopoulos and Stamenovic, 2006; Lazopoulos and Pirentis, 2007). They modelled the cell as a pre-stressed, isotropic, Mooney–Rivlin elastic material and performed analytical computations, finding that the stable preferential orientation is almost perpendicular to the strain direction. However, their model predicts that the final orientation angle increases with the magnitude of applied strain, which does not seem to be the case in all experiments as discussed in Section 2.1. Instead, experimental assays point towards a narrowing of the probability distribution for increasing strain. The model is then extended to account for the coexistence of symmetric orientations by considering a non-convex strain energy density function (Lazopoulos and Pirentis, 2007). Such a choice allows to obtain two symmetric oblique orientations, albeit the energy is quite non-standard for stress fibres (Deguchi et al., 2006). The same authors relax this assumption in a following work (Stamenovic et al., 2009), by focusing on an individual SF-FA assembly with linear elastic behaviour at the microscopic scale. It is shown that the emergence of stable oblique orientations requires the introduction of the chemical potential of the fibres, which has to be stress-dependent (Stamenovic et al., 2009). Moreover, the geometrical role of FAs in the reorientation process is underscored. Finally, in Pirentis et al. (2011) the effect of cytoskeletal fluidisation and resolidification is also taken into account.

To conclude, in a recent publication, Chatterjee et al. (2022) proposed a model based on the multiplicative decomposition of the deformation gradient for cell reorientation, where the cell is considered as a nonlinear elastic solid. In such a model, SFs can rotate and grow as a consequence of the deformation. Indeed, their reorientation vector $\mathbf{m}$ follows an elementary evolution law given by

$$\frac{d\mathbf{m}}{dt} = \frac{1}{\tau}\left[\mathbf{m}_{\text{target}} - (\mathbf{m}_{\text{target}} \cdot \mathbf{m})\mathbf{m}\right],$$

which enforces the fibres to preferentially align along the direction $\mathbf{m}_{\text{target}}$. The latter is taken as orthogonal to the uniaxial applied stretch, so it is implicitly assumed that such an orientation is always preferential for the SFs, which might not be the case for all experimental conditions. Instead, stress fibre growth is described by introducing a phenomenological growth tensor.
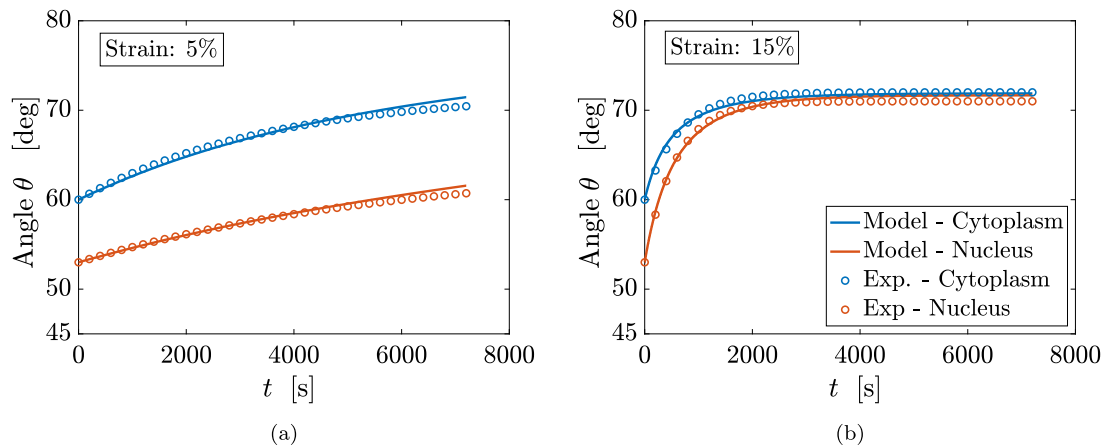
Fig. 13. Fitting of the model proposed in Ciambella et al. (2022) and summarised by Eq. (21) with experimental data taken from Roshanzadeh et al. (2020), for the reorientation of the cell cytoplasm (blue curves) and nucleus (red curves). The maximum applied strain is 5% in (a) and 15% in (b).

3.5. Viscoelasticity

Even though the equilibrium orientations obtained by means of the purely elastic approaches of the previous Subsection compare well with experimental data, the process of cell realignment is intrinsically viscoelastic. Indeed, as discussed in Section 2.1, the frequency of the applied cyclic deformation appears to influence the reorientation time, and also involves threshold effects. Moreover, in some cases, experiments have shown that the strain rate of the cyclic stretch, or equivalently the choice of different waveforms, might affect the reorientation of cells. These mechanisms cannot be captured by elastic models, which by their nature imply an instantaneous response, and call for the introduction of characteristic times or viscous dynamical processes.

Almost all the models that, to our knowledge, account for viscoelastic properties are based on descriptions at the microscale. Indeed, some of the frameworks for stress fibre modelling discussed in Section 3.1 embed viscosity in direct or indirect ways, taking into account that SFs have been shown experimentally to behave as viscoelastic cables (Kumar et al., 2006).

Just to mention some examples, the simple sarcomeric model of SFs by Kaunas et al. (2011) is certainly able to account for viscous-like effects. By considering the SF as a filament composed of actively contractile subunits in parallel, they derive an evolution equation for the force in each subunit, which features both an elastic contribution and a force relaxation due to myosin activity. Specifically, for high applied frequencies, the SF is unable to respond quickly enough to mechanical changes and the behaviour is almost elastic. Conversely, for low frequency, the SF manages to regulate its optimal force: these viscous-like effects related to acto-myosin sliding correlate well with differences due to frequency seen in experiments (see Section 2.1).

A similar approach is pursued by Chen et al. (2012), with emphasis on the intrinsic clocks of the cell and on the role of focal adhesions, and by Qian et al. (2013) and Lin et al. (2020), who considered a Maxwell-like viscoelastic model with an active force contribution. In the works by Kong et al. (2008) and Zhong et al. (2011), the cytoskeletal fibres were described by Kelvin–Voigt elements coupled with focal adhesions. The viscoelastic stress relaxation of SFs is instead modelled by Nagayama et al. (2012) using a seven-parameter spring-dashpot scheme, which features three different characteristic times. Such a description turns out to be able to fit their experimental curves for different waveforms and suggests that SFs avoid directions where they undergo compressive forces for too long times.

The cell dipole model by De and Safran (2008), De (2018) and Safran and De (2009) is also able to introduce a distinction in the outcomes between high and low frequency regimes. In their case, the relaxation

dynamics is postulated, highlighting a relation between the frequency and the characteristic time which is coherent with experimental data.

Instead, to the best of our knowledge, macroscopic viscoelasticity frameworks to describe the reorientation of cells under stretch are very few. Here, we mention the work by McEvoy et al. (2019), in which a nonlinear viscoelastic element composed of a spring in parallel with another spring and a dashpot is used to reproduce the passive mechanical behaviour of the cell cytoskeleton, in addition to its active counterpart. Focusing on the cell force generation during cyclic stretching and on acto-myosin dynamics, they are able to reproduce the experimental results by Wille et al. (2006). In particular, it is found that the maximum cell force increases in time at low amplitudes, while at high amplitudes force relaxation is observed. Reynolds and collaborators (Reynolds et al., 2020) adopted an analogous framework, with an additional component to represent the mechanics of the hydrogel wherein the cells are embedded. Their results are in agreement with experimental observations in 3D cultures, as described in Section 2.2, for uniaxially and biaxially constrained tissue constructs.

More recently, Lucci et al. (2021) introduced a viscoelastic model in a Continuum Mechanics framework to explain why, on the time scale of experiments, the reorientation phenomenon does not occur for small frequencies, for instance, as a consequence of the reorganisation of focal adhesions. The proposed model for the stress $\mathbb{T}(t|\theta)$ at time t given the history of orientations θ reads

$$\mathbb{T}(t|\theta) = \int_{-\infty}^{t} \frac{1}{\lambda} e^{-(t-\tau)/\lambda} \mathsf{C}_0(\theta(\tau))[\mathbb{E}(t) - \mathbb{E}(\tau)]\, d\tau\,, \qquad (23)$$

where $\mathsf{C}_0(\theta(\tau))$ is the elasticity tensor depending on the orientation direction θ at a past time τ and the exponential is the memory kernel (for more details on this type of models the reader can for instance refer to Astarita and Marrucci, 1974 for the isotropic case and to Pettermann and DeSimone, 2018; Pettermann et al., 2020 for the anisotropic case). Eq. (23) is then coupled with an equation for the evolution of θ, which is driven by the work done by the stress $\mathbb{T}$, namely,

$$\frac{d\theta}{dt}(t) = -\frac{1}{\eta} \frac{\partial \mathbb{T}}{\partial \theta}(t|\theta) : \mathbb{E}(t)\,, \qquad (24)$$

where η is a viscosity coefficient and $\mathbb{E}$ is the strain tensor which, as in the experiments, represents a periodic deformation externally imposed to the specimen. Then, it is shown that, in the high frequency regime, the response is elastic and the cell reorients as predicted by the models in Section 3.4, trying to minimise the energy. Conversely, in the low frequency regime, in which the period of the cyclic strain imposed to the specimen is much longer than the characteristic time of cell relaxation, the reorientation process becomes viscous. The cell therefore adapts to the imposed strain and does not reorient significantly on the time scale of the experiment.
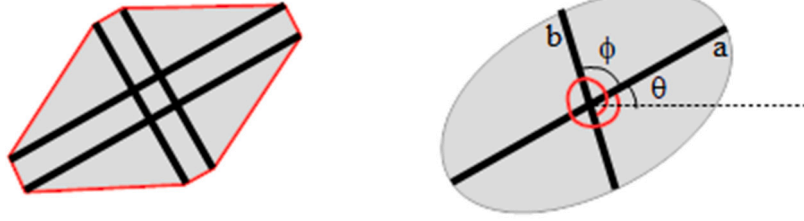
Fig. 14. Tensegrity models with two pairs of perpendicular struts (thick black lines), like those used in Mao et al. (2021) and Xu et al. (2016, 2018), on the left, and with two struts connected by a torsional spring between the two struts, as in Colombi et al. (2023), on the right.

3.6. Tensegrity models

In order to describe cell reorientation, Xu and coworkers (Xu et al., 2016, 2018), and then Mao et al. (2021), used tensegrity-like models. Specifically, as sketched in Fig. 14a, such models schematise the cells as formed by two parallel elastic struts along the orientation axis and two other struts perpendicular to them. A string connecting the ends of the struts is also formally considered, but then neglected in the computation. The energy of the system is then evaluated, but unfortunately there are some flaws in the computation of the work done by the applied force in addition to some incorrect signs (see their Eqs. (13) and (18)), that are a posteriori adjusted. Anyway, the energy discussed is coherent with that in Section 3.4. This allows to recover both equilibrium orientations and the ordinary differential equation for the temporal evolution of the orientation.

Along the same spirit, with the aim of focusing on the effect of substratum stiffness (see Section 2.1.2), Colombi et al. (2023) schematised the cell as formed by two elastic elements that model the behaviour of stress fibre/focal adhesion complexes in the main and transversal orientations as in Fig. 14b. The two elements are hinged at their centre through a torsional elastic spring which mimics the action of cross-linking molecules among stress fibres that resist to shear. The remodelling equation determining the evolution of the orientation of the cell is then proved to be

$$\frac{h}{k_a L_a^2} \frac{d\theta}{dt} = \frac{2\hat{k}_s^2}{(1+\hat{k}_s)^2} \varepsilon^2(t)(1+r)^2 \left[A_1(\hat{k}_s)\cos^2\theta - A_2(\hat{k}_s) - \frac{A_3(\hat{k}_s)}{1+r} \right] \sin\theta\cos\theta,$$

(25)

where A_i with $i = 1, 2, 3$ are suitable dimensionless functions of $\hat{k}_s = k_s/k_a$, i.e. the ratio of the elastic modulus of the substratum k_s and the one of the element along the main cell orientation k_a. In addition, L_a is the size of the cell along its main direction, and h is related to the characteristic time for stress fibre and focal adhesion remodelling dynamics.

In the limit case of a stiff substratum, the model reduces to the ones discussed in Section 3.4. On the other hand, the inclusion of substratum compliance has two effects that are coherent with experiments. The first one is that softer substrata lead to much slower evolutions. This is also evident from the presence of the term $\hat{k}_s^2$ in Eq. (25). The second one is that, when the substratum is soft enough, equilibrium configurations with cell axis parallel to the main stretching direction may become stable, as seen in experiments (Terracio et al., 1988; Thodeti et al., 2009).

In fact, it is found that, for any fixed biaxiality ratio r, the stability character of the equilibria depends on the mechanical parameters contained in the functions $A_i(\hat{k}_s)$ and therefore on $\hat{k}_s$, with a stability switch from supercritical to subcritical for softer substrata. In terms of substratum stiffness, this means that the presence of a stable oblique orientation is favoured by sufficiently large substrate stiffness (corresponding to the region above the upper orange surface in Fig. 15a),

while the subcritical scenario characterised by the stability of parallel and perpendicular orientations is favoured when the substrate softens (corresponding to the region between the orange surfaces in Fig. 15a). In Fig. 15, $\hat{k}_b = \frac{k_b}{k_a}$ and $\hat{k}_\theta = \frac{2k_\theta}{k_q L_a^2}$ respectively compare the elastic modulus in the direction perpendicular to the main cell axis and the response to shear with the elastic modulus along the cell axis.

For instance, referring to Fig. 15b, obtained fixing $\hat{k}_\theta = 0.4$ in addition to the biaxiality ratio r, focusing on the region $\hat{k}_b > \hat{k}_\theta$, the stable equilibrium angle first decreases from a value slightly above $\frac{\pi}{4}$ to a value below $\frac{\pi}{4}$. Decreasing further $\hat{k}_s$, the stable equilibrium angle is the one along the principal strain direction, with the oblique equilibrium that becomes unstable. A further softening of the substrate then leads to the stability of both the parallel and perpendicular configuration, still with an unstable oblique equilibrium.

3.7. Statistical mechanics

To conclude the review about mathematical models, we briefly mention some works based on classical tools of statistical mechanics that allow to describe the statistical distribution of the orientations of the cells. Indeed, as shown in Figs. 4 and 3(b), the biological phenomenon under study is intrinsically affected by a certain degree of randomness and, because of the already mentioned possible symmetries of the system, measurements of the frequencies of the orientations are reported over $\left[0, \frac{\pi}{2}\right]$ or $[0, \pi]$. Almost all the approaches introduced so far work in a deterministic framework and recover the behaviour of the average orientation in the transient or at equilibrium. However, an interesting issue is also the determination of the probability density function $f = f(\theta)$ (over $\left[0, \frac{\pi}{2}\right]$ or $[0, \pi]$, respectively) of the orientations of the cells, that allows for a complete statistical description. This is typically carried out, in the field of statistical mechanics, by defining a microscopic dynamics for the orientation θ and by deriving subsequently an evolution equation for a probability density function $f = f(t, \theta)$ describing the statistical distribution of the orientations of cells following the aforementioned microscopic process. We also highlight the fact that if f is considered on the symmetry interval according to the given experimental set-up, then f is unimodal and the linear and circular average coincide.

Kemkemer and coauthors (Kemkemer et al., 2006, 1999) provide one of the first formal treatments of this problem: they model the evolution of the orientation of a cell by means of an automatic controller, i.e. an ODE describing the temporal evolution of the single-cell orientation with an empirical forcing term that has the desired symmetry, plus a random noise. The resulting stochastic differential equation (SDE) allows to obtain, as a Fokker–Planck forward equation, the evolution equation of the probability density function f. The stationary state of the resulting Fokker–Planck equation is an exponential of a doubly-wrapped cosine, that is a Boltzmann-like distribution. In particular, they compare the analytical findings with experimental results and
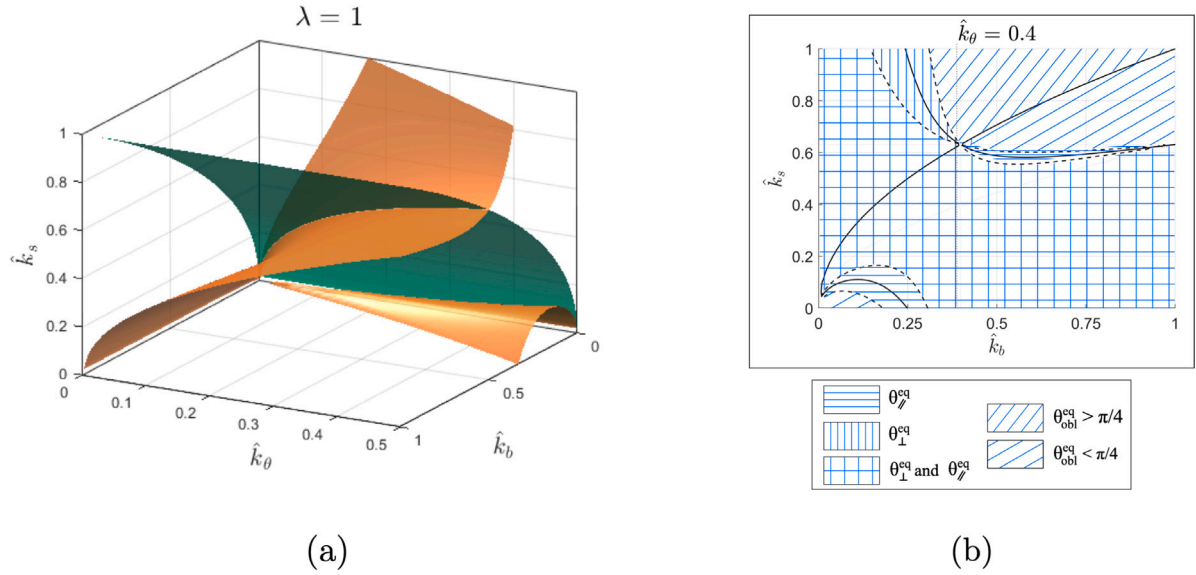
Fig. 15. (a) Surfaces delimiting the different bifurcation scenarios. In particular, the equilibrium orientation is stable above the upper surface and below the lower surface and unstable in between them, corresponding to a supercritical bifurcation in the former region and subcritical in the latter. (b) Cross section of the space of parameters for $\hat{k}_\theta = 0.4$. The stable configurations for $r = 0.5$ are sketched.

show that the Boltzmann-like distribution can describe cell orientations on curved substrata.

Similarly and coherently with other already mentioned deterministic models, in many works the evolution of the cell orientation θ is related to a linear elastic energy $\mathcal{U}$ through

$$\frac{d}{dt}\theta \propto -\frac{\partial}{\partial \theta}\mathcal{U}. \tag{26}$$

This leads many authors to postulate a Boltzmann probability density function f as

$$f(t,\theta) \propto e^{-\frac{\mathcal{U}(\theta)}{kT}},$$

that is coherent with the fact that the cells' orientation evolves according to Eq. (26). Then, all the efforts lie in the modelling of the energy $\mathcal{U}$ of the system and of its temperature T. In this respect, De and collaborators (Safran and De, 2009; De, 2018) and Qian et al. (2013) implemented some non-deterministic effects in their models, mainly dealing with the association and dissociation processes of SFs under the action of stretch. In particular, in the work by Safran and De (2009) the authors describe the cell as a reorienting dipole subject to a periodic stretch and model the distribution of the orientations as a Boltzmann distribution with a competition between the force determining the free energy of the dipole and the effective temperature. Faust et al. (2011) use this distribution assuming an energy corresponding to the strain avoidance hypothesis. Also Mao et al. (2021) consider a Boltzmann-like distribution with an energy that is the sum of three contributions given by the work done by focal adhesions, by the pulling force and by the elastic potential energy of bars in the tensegrity structure, that however, as discussed in Section 3.6 presents a flaw. In a similar spirit, the stochastic nature of SF formation and activation is included through proper probability functions in the work by Hsu et al. (2009, 2010), Kaunas et al. (2011) and by Tondon et al. (2012), which were all discussed before.

Always in the field of statistical mechanics, recently, Loy and Preziosi (2023) have proposed a kinetic theory approach in order to tackle this problem. The starting point is the Ito process

$$d\theta = -\frac{\varepsilon^2}{\tau_\theta}\frac{\partial \bar{U}}{\partial \theta}dt + \sqrt{\frac{\sigma^2}{\tau_\theta}}dW_t \tag{27}$$

where $dW_t = \sqrt{t}\xi$, being W_t a Wiener process, σ takes into account the stochastic fluctuations related to cell behaviour, and $\bar{U}$ is the strain independent dimensionless energy, e.g., $\mathcal{U}_{cell}/(K_\parallel \varepsilon^2)$ where $\mathcal{U}_{cell}$ is defined in Eq. (17) and $K_\parallel$ measures the elastic response to deformations along the main cell orientation axis.

The forward equation of $f = f(t,\theta)$ is

$$\frac{\partial}{\partial t}f(t,\theta) = \frac{\varepsilon^2}{\tau_\theta}\frac{\partial}{\partial \theta}\left(\frac{\partial \bar{U}}{\partial \theta}(\theta)f(t,\theta)\right) + \frac{1}{2\tau_\theta}\frac{\partial^2}{\partial \theta^2}\left(\sigma^2 f(\theta,t)\right). \tag{28}$$

From Eq. (28) it can be readily observed that an increase in the applied strain ε would increase the importance of the drift term with respect to diffusion. Vice versa, decreasing excessively ε would lead to a diffusion dominated problem, in which random noise covers the re-orientation tendency expressed by the drift term. This is also evident by looking at the stationary state of Eq. (28) that writes

$$f^\infty(\theta) = C\exp\left(-\frac{2\varepsilon^2\bar{U}(\theta)}{\sigma^2}\right) \tag{29}$$

where C is a normalisation constant. In fact, it presents maxima (resp. minima) corresponding to minima (resp. maxima) of $\bar{U}$ and peaks up when ε increases. The distribution postulated by Faust et al. (2011) is recovered by taking

$$\bar{U}(\theta) = [(1+r)\cos^2\theta - r]^2 \approx \frac{(I_4-1)^2}{4\varepsilon^2},$$

and that by Mao et al. (2021) by taking

$$\bar{U}(\theta) = \xi_1\cos^4\theta - \xi_2\sin^4\theta,$$

that can be for instance obtained as a suitable combination of I_4 with I_6 and/or I_8, then linearised. Moreover, it is found that the distributions postulated by Faust et al. (2011) and by Mao et al. (2021) can be recovered as particular cases.

The emergence of statistical distributions with a double peak is also discussed by Moriel et al. (2022) and by Gérémie et al. (2022). Both these groups extended the evolution Eq. (15) by adding a random noise term with zero mean and unit variance, and found results coherent with Loy and Preziosi (2023). As mentioned in Section 3.5, the inclusion of viscoelastic effects leads to the same results in the high frequency regime. On the other hand, in the low frequency regime, a different dimensional analysis can be performed and leads ε^2 to be formally replaced by $\varepsilon^2\tau\omega$, so that the effective dimensionless diffusion
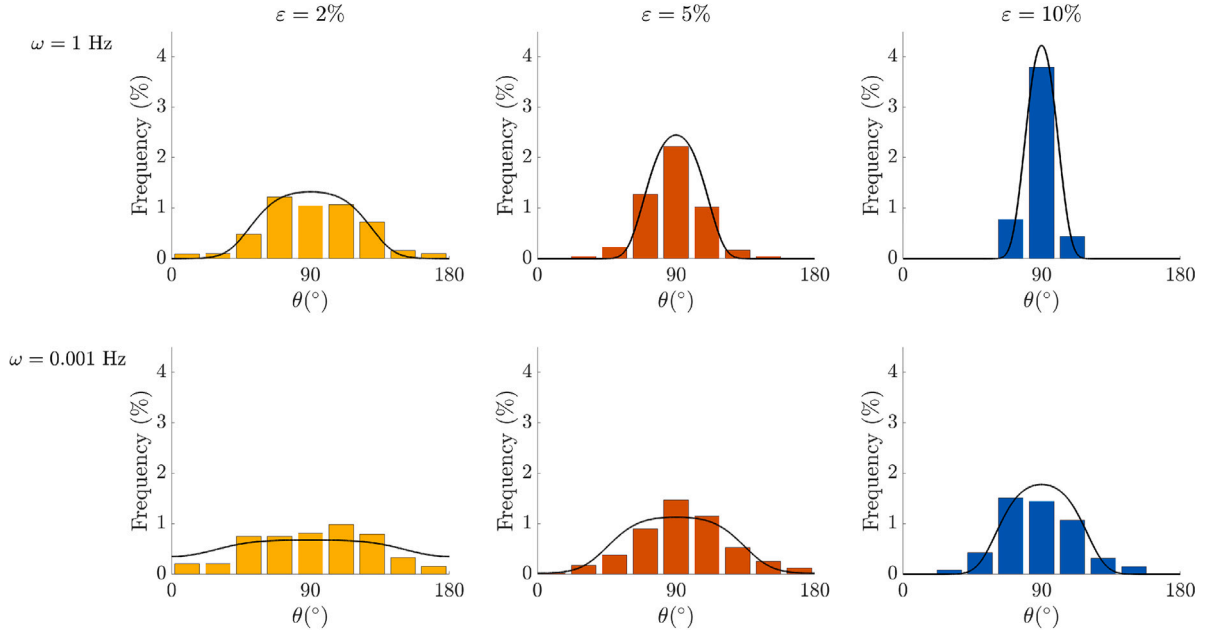
Fig. 16. Equilibrium distributions (29) changing ω and ε, while $\sigma = 0.2$ everywhere. The parameter $\varepsilon = 2\%, 5\%, 10\%$ (first, second and third columns, respectively) varies according to the experimental set-up giving rise to decreasing values of $\bar{\sigma}^2 = \frac{\sigma^2}{2\varepsilon^2}$ in the first row and $\bar{\sigma}^2 = \frac{\sigma^2}{2\varepsilon^2\tau\omega}$ with $\lambda = 100\,\text{s}$ in the second row.

coefficient is $\bar{\sigma}^2 = \sigma^2/(2\tau\omega\varepsilon^2)$. This shows that increasing ω leads to more peaked distributions. In Fig. 16, in order to replicate the data reported by the histograms of Mao et al. (2021), f^∞ given by Eq. (29) is plotted setting $\sigma = 0.2$ and varying ε and ω. When $\omega = 1\,\text{Hz}$ (top row of Fig. 16), corresponding to a high frequency regime, an increase in the strain amplitude, coherently with the fact that $\bar{\sigma}^2 = \frac{\sigma^2}{2\varepsilon^2}$ (so, it goes like ε^{-2}) leads to more peaked distributions that fit quite well the experimental ones. For $\omega = 0.001\,\text{Hz}$ (bottom row of Fig. 16), corresponding to a low frequency regime, $\bar{\sigma}^2 = \frac{\sigma^2}{2\varepsilon^2\tau\omega}$ is used. Also in this case, the distributions peak up increasing the strain amplitudes and the theoretical results compare well with the experimental results, notwithstanding viscoelastic effects are simply included through a modification of $\bar{\sigma}$ that is valid in the low frequency regime. On the other hand, for a fixed ε at the different ω's, simulations give more peaked distributions for higher frequencies (see Fig. 16 all columns read from top to bottom).

The kinetic theory approach is then developed by considering a Boltzmann-like kinetic equation for the probability density function in which the microscopic dynamics for the evolution of the orientation angle θ is described by the following rule, specifying the new angle θ' after transition:

$$\theta' = \theta - \gamma_i \varepsilon^2 \frac{\partial \bar{U}}{\partial \theta} + \sqrt{\gamma_i \sigma^2}\xi \quad \mathrm{mod}(\pi), \tag{30}$$

where ξ is a Gaussian random variable with zero mean and unitary variance, and $\gamma_i \ll 1$ is a small parameter describing how much cells reorient at each transition. The application of the quasi-invariant direction limit (that is a classical tool of kinetic theory) to the Boltzmann-like integro-differential equation joined with (30) allows to derive (28).

Coming to a comparison of the model (28) with the experimental results, Fig. 17 reports the result of a Montecarlo simulation of the microscopic process (30) in the quasi-invariant regime allowing to approximate (28). In Fig. 17 the results are compared with experimental data reported in the work by Hayakawa et al. (2001) for $\varepsilon = 20\%$, $r = 0.4$ and $\omega = 1\,\text{Hz}$ (see the coloured bars). In particular, in the work by Hayakawa et al. (2001) it was found that at $t = 1\,\text{h}$ the average orientation is 52.8°, while at $t = 3\,\text{h}$, when more than the 80% of the cells are oriented at angles of 50°–80°, the average orientation is 62.02°.
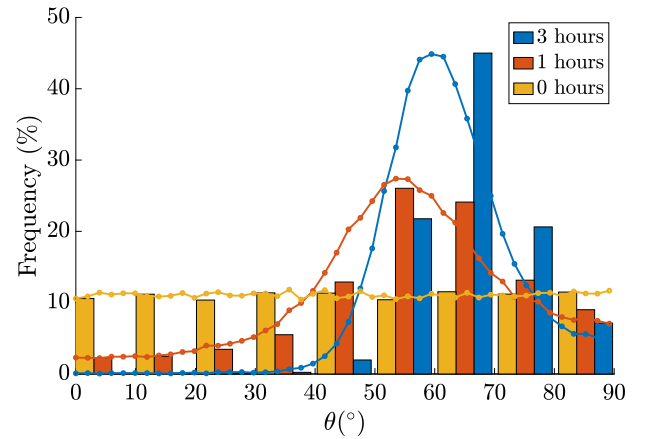

Fig. 17. Comparison of the evolution of the probability density function obtained by performing a Montecarlo simulation of Eq. (30) with the experimental data reported in Hayakawa et al. (2001). In particular, $\varepsilon = 20\%$ and $r = 0.4$. Bars refer to experimental data at $t = 0, 1, 3$ h, respectively in yellow, red and blue. Curves are the recovered probability density functions at $t = 0, 1, 3$ h. Solution for $\theta_{eq} \approx 61°$, $\sigma \approx 0.04$, and $\tau_\theta \approx 0.18\,\text{s}$.

Using Eq. (18) and for $\mathcal{K}$ the value suggested in Livne et al. (2014), the minimum of the elastic energy is attained at $\theta_{eq} \approx 61°$. The value of σ is set to $\sigma \approx 0.04$ so that the mean of the distribution function over $\left[0, \frac{\pi}{2}\right]$ is $\bar{\theta}_\ell = 62.2°$. After 1 hour the average orientation is 54.6° and after 3 h it is 62.04° and the 85% of the cells is oriented at angles of 50°−80°.

We also cite in this Section the work by Buskermolen et al. (2019), who deal with a Statistical Mechanics framework for cell homeostasis. Such a description turns out to be appropriate for the modelling of cell alignment on micropatterned substrates as a function of stripe width.

Finally, a very recent work by Das et al. (2022) extended the Statistical Mechanics framework proposed in the work by Shishvan et al. (2018) to the cell cyclic straining experiment. The main outcomes of such a model involve the decoupling between the SFs and cell morphology dynamics. The results reproduce quite well the experimental
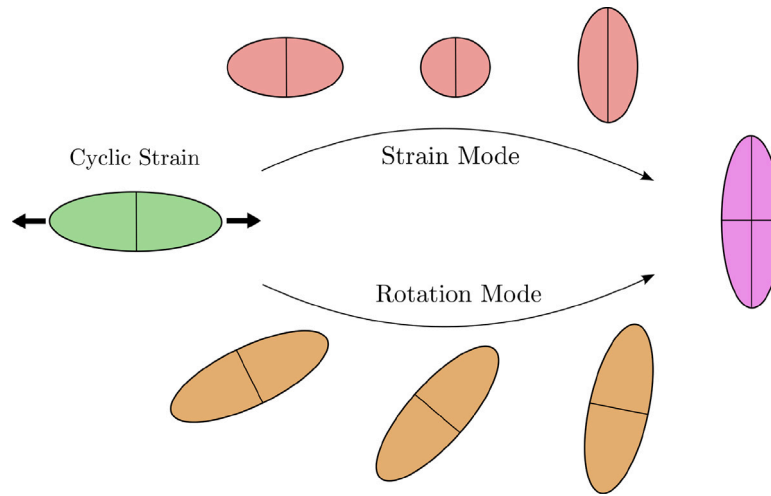
Fig. 18. Possible modes of cell reorientation under cyclic strain. In the strain mode, the cell disassembles the stress fibres aligned in the stretching direction, becomes rounded, and then rebuilds them in the newly preferential direction. Instead, in the rotation mode, the cell remains elongated and actually undergoes a rotation of its major axis. According to the Statistical Mechanics model in Das et al. (2022), the latter seems to be the preferable process.
Source: Redrawn from Das et al. (2022).

data for strains of high frequency and for the case $r = 0$, in which the cell is expected to align perpendicularly. However, the model predicts that in general cells preferentially orient at the angle that minimises the strain rate, following again Eq. (6). An intriguing result proposed in the work by Das et al. (2022) concerns instead the manner whereby cell reorientation towards the preferred direction happens. In fact, experimental results do not appear to fully clarify whether the cell follows a *strain mode*, firstly becoming rounded and then elongating towards the new direction, or a *rotation mode*, in which the cell elliptic body actually rotates (see Fig. 18). Remarkably, the simulations of the statistical framework in the work by Das et al. (2022) strongly suggest that the rotation mode is the preferable process.

3.8. Reorientation as an optimal control problem

To our knowledge, the first to conceive cell reorientation as a control problem were Kemkemer and coauthors (Kemkemer et al., 2006, 1999). In the work by Loy and Preziosi (2023) it is assumed that, in the reorientation process, the cell rotates in an optimal way, i.e. in order to minimise a certain energy functional (see Section 3.4). This can be rewritten as a control problem, assuming that the dynamics of the cell is governed by the energy functional that tends to be minimised and the cell varies its orientation by an angle ψ_{opt} that minimises a certain cost functional $\mathcal{J}$. In particular, this is implemented in the Boltzmann kinetic framework introduced in Section 3.7, describing the evolution of f for orientation angles by performing the following dynamics:

$$\theta' = \theta + \nu\psi_{opt}, \quad \psi_{opt} = \text{argmin}_\psi \mathcal{J}(\psi), \tag{31}$$

where

$$\mathcal{J}(\psi) = \nu\frac{\psi^2}{2} + \langle q(\theta') \rangle,$$

being ν a coefficient and q a proper function of θ. It is then proved that Eq. (28) is recovered if

$$q = \varepsilon^2 \bar{U}. \tag{32}$$

On the other hand, if the following classical rule is adopted:

$$q(\theta') = \frac{\varepsilon^2}{2}[\theta' - \hat{\theta}(\theta)]^2, \tag{33}$$

with $\hat{\theta}(\theta)$ modelled in such a way that if θ is already close to an equilibrium orientation, then it is more likely to stay there, then the

equilibrium distribution is given by

$$f^\infty(\theta) = C \exp\left(\int_0^\theta \frac{2\varepsilon^2}{\sigma_c^2}[\hat{\theta}(\theta) - \theta]d\theta\right), \tag{34}$$

where C is the normalisation constant and σ_c is a measure of the stochastic fluctuation.

Fig. 19 gives a comparison of the stationary distributions given by Eqs. (29) and (34) with the experimental data by Faust et al. (2011), obtained applying different stretching amplitudes, namely $\varepsilon = 8.4\%$, 11.8%, and measuring a biaxiality ratio $r = 0.15$. Taking again $\mathcal{K} = 1.26$, as suggested in the work by Livne et al. (2014), the minimum elastic energy and therefore the mode is obtained at $\theta_{eq} \approx 79°$. The value of σ_c is set in such a way that the mean orientation evaluated in $\left[0, \frac{\pi}{2}\right]$ is the same as in Faust et al. (2011).

Fig. 20 compares the results obtained by Jungbauer et al. (2008) with the mean of the distribution function obtained by integrating Eq. (31). In the experiment, the substrate stretching, with $\omega = 2\,\text{Hz}$, $r = 0.194$ and $\varepsilon = 8\%$, is stopped after 3000 s. Hence, the contribution of the drift term vanishes and only the random term is active leading to a recovery phase towards a uniform distribution.

4. Conclusions and perspectives

In this article, we have provided a thorough review of the experimental and modelling literature about the cellular response to mechanical cues. In particular, we analysed the phenomenon of cell reorientation under cyclic stretching of the substrate, which is extremely relevant in a number of tissues in physiological conditions: blood vessels, the heart, the lungs, the intestine, and muscles are all constantly subjected to periodic deformations, to name but a few. Moreover, understanding how a cell orients as a reaction to environmental alterations is extremely relevant in tissue engineering, where the aim is to build artificial tissues in a faithful way, and also in medicine, since some pathologies appear related to issues in cell mechanotransduction (Ingber, 2003).

We summarised the main features of the numerous experiments performed from the 1980s until today, trying to capture the relevant factors that are involved in cell reorientation on smooth 2D substrates and in 3D matrices. In particular, on smooth 2D substrates, cells reorient obliquely or perpendicularly to the main stretching direction, with a key role played by the amplitude, the frequency, the biaxiality of the periodic deformation, as well as by the substrate stiffness. In
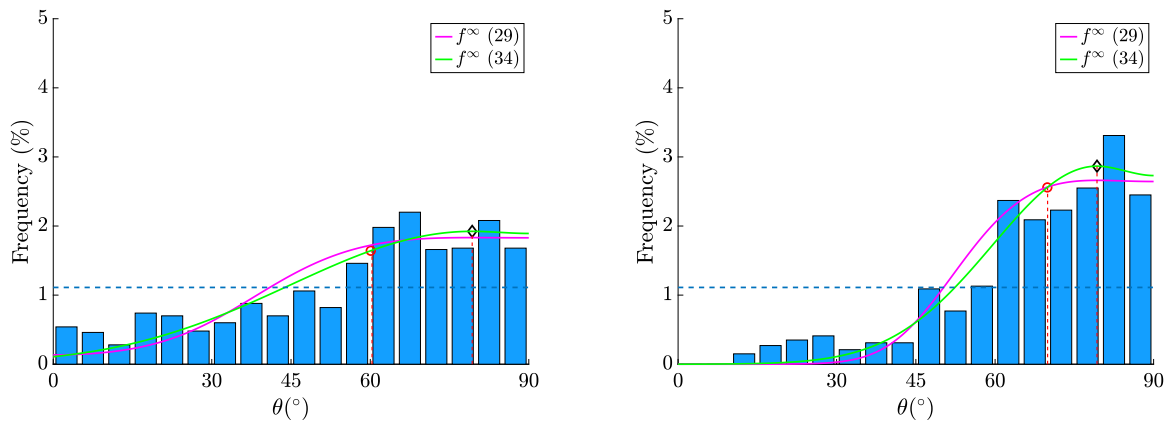
Fig. 19. Equilibrium distributions f^∞ computed as in Eqs. (29) (purple line) and (34) (green line) for $\varepsilon = 8.4\%$ (on the left) and $\varepsilon = 11.8\%$ (on the right), compared with data from Faust et al. (2011) represented by light blue bars. The red circles represent the average circular orientation and the black diamonds represent θ_{eq}.
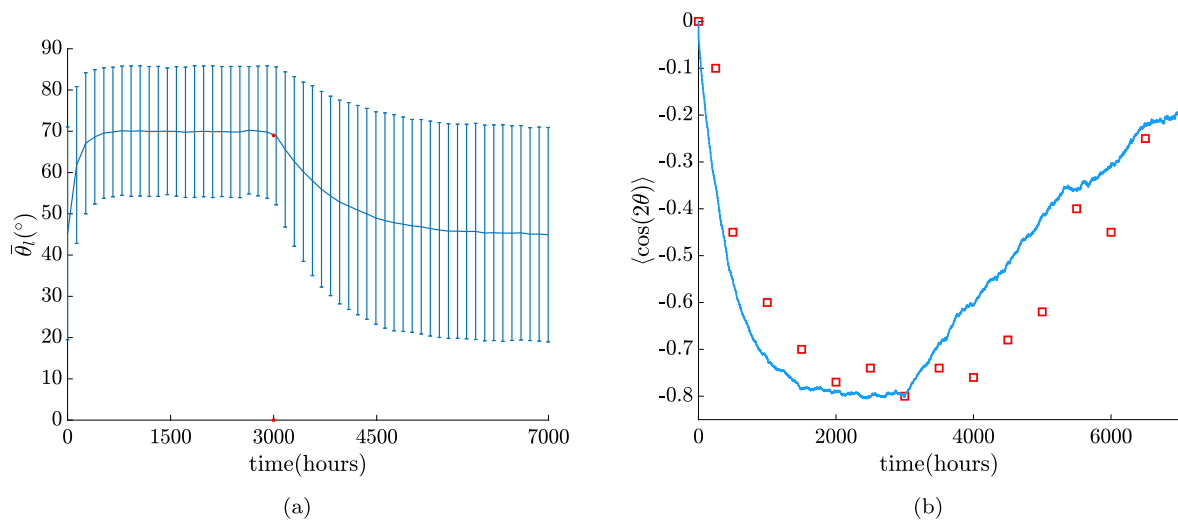
Fig. 20. Temporal evolution of the mean of the orientation distribution. In (a) the mean of the orientation angle, with standard deviation, is the one reported in Jungbauer et al. (2008). The parameter values are $\tau_\theta = 6.6\,\text{s}$, $\mathcal{K} = 1.26$ and $\sigma = 1.6$. After 3000 s stretching stops and cells tend to reorient uniformly over the angle. In (b) the same mean is reported in terms of its $\cos 2\theta$ for a more direct comparison with the experimental data (red squares) reported in Jungbauer et al. (2008).

3D matrices (as well as on 2D grooved substrates, not analysed in this review), instead, contact guidance comes into play and the behaviour of cells under cyclic strains becomes more involved.

For what concerns the mathematical models, we have underscored the main approaches and theoretical features employed by different groups to tackle the problem of predicting the final orientation of a cell as a consequence of a mechanical periodic stimulus. Starting from the first frameworks, which suggested that either strain or stress avoidance were the preferential mechanisms, we have reviewed some more recent results that are based on the minimisation of appropriate elastic energies, showing a very good agreement with experimental data. Finally, we presented mathematical models grounded on Statistical Mechanics tools, which account for the randomness of the cell reorientation process, and tensegrity-like models, which are able to include the compliance of the substrate.

To conclude, a mathematical understanding of mechanotransduction and cellular reaction to mechanical cues is still not fully developed. Indeed, there are several open problems concerning the reorientation of the cell cytoskeleton under periodic deformations. From the experimental point of view, it would be important to develop assays which are able to perform biaxial and consistent deformations, to get some precise insight into the effect of different patterns of tension and compression on cells. In addition, the application of static or step stretches should

be investigated in more detail, since the results in such cases are still debated.

On the mathematical modelling side, first of all it would be relevant to explicitly feature the adhesion between cells and substrate. It is known that the link between a cell and its environment, due to focal adhesions, is fundamental in the transduction of mechanical signals both outside-in and inside-out. Therefore, even if the modelling becomes more complicated, it might be worth to investigate attachment and detachment effects. This purpose should probably be pursued by considering a more detailed description of viscoelasticity, for instance accompanied by a multiplicative decomposition of the deformation gradient. Moreover, the role of microtubules in reorientation is not fully elucidated, and mathematical models accounting for them could probably be useful to better understand their involvement. Finally, a link between the microscopic scale, where transduction of the mechanical signal happens as a chemical process, and the macroscopic cytoskeletal reorganisation should be drawn, also supported by experimental evidence.

Declaration of competing interest

The authors declare that they have no known competing financial interests or personal relationships that could have appeared to influence the work reported in this paper.

References

Abbott, R., Howe, A., Langevin, H., Iatridis, J., 2012. Live free or die: Stretch-induced apoptosis occurs when adaptive reorientation of annulus fibrosus cells is restricted. Biochem. Biophys. Res. Commun. 421, 361–366.

Abeyaratne, R., Puntel, E., Tomassetti, G., 2022. An elementary model of focal adhesion detachment and reattachment during cell reorientation using ideas from the kinetics of wiggly energies. J. Elasticity.

Ahmed, W., Wolfram, T., Goldyn, A., Bruellhoff, K., Rioja, B., Moller, M., Spatz, J., Saif, T., Groll, J., Kemkemer, R., 2010. Myoblast morphology and organization on biochemically micro-patterned hydrogel coatings under cyclic mechanical strain. Biomaterials 31, 250–258.

Alberts, B., Johnson, A., Lewis, J., Raff, M., Roberts, K., Walter, P., 2008. Molecular Biology of the Cell, fifth ed. Garland Science.

Asano, S., Ito, S., Morosawa, M., Furuya, K., Naruse, K., Sokabe, M., Yamaguchi, E., Hasegawa, Y., 2018. Cyclic stretch enhances reorientation and differentiation of 3D culture model of human airway smooth muscle. Biochem. Biophys. Rep. 16, 32–38.

Astarita, G., Marrucci, G., 1974. Principles of Non-Newtonian Fluid Mechanics. McGraw-Hill.

Atcha, H., Davis, C., Sullivan, N., Smith, T., Anis, S., Dahbour, W., Robinson, Z., Grosberg, A., Liu, W., 2018a. A low-cost mechanical stretching device for uniaxial strain of cells: A platform for pedagogy in mechanobiology. J. Biomech. Eng. 140, 081005.

Atcha, H., Meli, V., Davis, C., Brumm, K., Anis, S., Chin, J., Jiang, K., Pathak, M., Liu, W., 2018b. Crosstalk between CD11b and Piezo1 mediates macrophage responses to mechanical cues. Front. Immunol. 140, 689397.

Barron, V., Brougham, C., Coghlan, K., McLucas, E., O'Mahoney, D., Stenson-Cox, C., McHugh, P., 2007. The effect of physiological cyclic stretch on the cell morphology, cell orientation and protein expression of endothelial cells. J. Mater. Sci. Mater. Med. 18, 1973–1981.

Bellows, C., Melcher, A., Aubin, J., 1982. Association between tension and orientation of periodontal ligament fibroblasts and exogenous collagen fibres in collagen gels in vitro. J. Cell Sci. 58, 125–138.

Bischofs, I., Schwarz, U., 2003. Cell organization in soft media due to active mechanosensing. Proc. Natl. Acad. Sci. USA 100, 9274–9279.

Boccafoschi, F., Bosetti, M., Gatti, S., Cannas, M., 2007. Dynamic fibroblast cultures: Response to mechanical stretching. Cell Adhes. Migr. 1, 124–128.

Boerboom, R., Rubbens, M., Driessen, N., Bouten, C., Baaijens, F., 2008. Effect of strain magnitude on the tissue properties of engineered cardiovascular constructs. Ann. Biomed. Eng. 36 (2), 244–253.

Bono, N., Pezzoli, D., Levesque, L., Loy, C., Candiani, G., Fiore, G., Mantovani, D., 2016. Unraveling the role of mechanical stimulation on smooth muscle cells: A comparative study between 2D and 3D models. Biotechnol. Bioeng. 113, 2254–2263.

Buck, R., 1979. The longitudinal orientation of structures in the subendothelial space of rat aorta. Am. J. Anat. 156, 1–14.

Buck, R., 1980. Reorientation response of cells to repeated stretch and recoil of the substratum. Exp. Cell Res. 127, 470–474.

Buck, R., 1983. Behaviour of vascular smooth muscle cells during repeated stretching of the substratum in vitro. Atherosclerosis 46, 217–223.

Buskermolen, A., Suresh, H., Shishvan, S., Vigliotti, A., DeSimone, A., Kurniawan, N., Bouten, C., Deshpande, V., 2019. Entropic forces drive cellular contact guidance. Biophys. J. 116, 1994–2008.

Cha, J., Park, S.-N., Noh, S., Suh, H., 2006. Time-dependent modulation of alignment and differentiation of smooth muscle cells seeded on a porous substrate undergoing cyclic mechanical strain. Artif. Org. 30 (4), 250–258.

Chatterjee, A., Kondaiah, P., Gundiah, N., 2022. Stress fiber growth and remodeling determines cellular morphomechanics under uniaxial cyclic stretch. Biomech. Model. Mechanobiol. 21, 553–567.

Chen, B., Kemkemer, R., Deibler, M., Spatz, J., Gao, H., 2012. Cyclic stretch induces cell reorientation on substrates by destabilizing catch bonds in focal adhesions. PLoS One 7, e48346.

Chen, Y., Pasapera, A., Koretsky, A., Waterman, C., 2013. Orientation-specific responses to sustained uniaxial stretching in focal adhesion growth and turnover. Proc. Natl. Acad. Sci. USA 110, E2352–E2361.

Chen, K., Vigliotti, A., Bacca, M., McMeeking, R., Deshpande, V., Holmes, J., 2018. Role of boundary conditions in determining cell alignment in response to stretch. Proc. Natl. Acad. Sci. USA 115 (5), 986–991.

Ciambella, J., Lucci, G., Nardinocchi, P., Preziosi, L., 2022. Passive and active fiber reorientation in anisotropic materials. Internat. J. Engrg. Sci. 176, 103688.

Collinsworth, A., Torgan, C., Nagda, S., Rajalingam, R., Kraus, W., Truskey, G., 2000. Orientation and length of mammalian skeletal myocytes in response to a unidirectional stretch. Cell Tissue Res. 302, 243–251.

Colombi, A., Preziosi, L., Scianna, M., 2023. Modelling cell orientation under stretch: The effect of substrate elasticity. http://dx.doi.org/10.1007/s11538-023-01180-1,

Dartsch, P., Betz, E., 1990. Cellular and cytoskeletal response of vascular cells to mechanical stimulation. In: Planck, H., Dauner, M., Renardy, M. (Eds.), Medical Textiles for Implantation. Springer, Berlin, Heidelberg, pp. 193–218.

Dartsch, P., Hammerle, H., 1986. Orientation response of arterial smooth muscle cells to mechanical stimulation. Eur. J. Cell Biol. 41, 339–346.

Dartsch, P., Hammerle, H., Betz, E., 1986. Orientation of cultured arterial smooth muscle cells growing on cyclically stretched substrates. Acta Anatomica 125, 108–113.

Das, S., Ippolito, A., McGarry, P., Deshpande, V., 2022. Cell reorientation on a cyclically strained substrate. PNAS Nexus 1, 1–15.

De, R., 2018. A general model of focal adhesion orientation dynamics in response to static and cyclic stretch. Commun. Biol. 1, 81.

De, R., Safran, S., 2008. Dynamical theory of active cellular response to external stress. Phys. Rev. E 78, 031923–031940.

De, R., Zemel, A., Safran, S., 2008. Do cells sense stress or strain? Measurement of cellular orientation can provide a clue. Biophys. J. 94, L29–L31.

De, R., Zemel, S., 2007. Dynamics of cell orientation. Nat. Phys. 3, 655–659.

De Jonge, N., Kanters, F., Baaijens, F., Bouten, C., 2013. Strain-induced collagen organization at the micro-level in fibrin-based engineered tissue constructs. Ann. Biomed. Eng. 41 (4), 763–774.

Deguchi, S., Ohashi, T., Sato, M., 2006. Tensile properties of single stress fibers isolated from cultured vascular smooth muscle cells. J. Biomech. 39, 2603–2610.

Deibler, M., Spatz, J., Kemkemer, R., 2011. Actin fusion proteins alter the dynamics of mechanically induced cytoskeleton rearrangement. PLoS One 6, e22941.

Deshpande, V., McMeeking, R., Evans, A., 2006. A bio-chemo-mechanical model for cell contractility. Proc. Natl. Acad. Sci. USA 103, 14015–14020.

Deshpande, V., McMeeking, R., Evans, A., 2007. A model for the contractility of the cytoskeleton including the effects of stress-fibre formation and dissociation. Proc. R. Soc. Lond. Ser. A Math. Phys. Eng. Sci. 463, 787–815.

Faust, U., Hampe, N., Rubner, W., Kirchgessner, N., Safran, S., Hoffmann, B., Merkel, R., 2011. Cyclic stress at mHz frequencies aligns fibroblasts in direction of zero strain. PLoS One 6, e28963.

Feng, Z., Wagatsuma, Y., Kikuchi, M., Kosawada, T., Nakamura, T., Sato, D., Shirasawa, N., Kitajima, T., Umezu, M., 2014. The mechanisms of fibroblasts-mediated compaction of collagen gels and the mechanical niche around individual fibroblasts. Biomaterials 35, 8078–8091.

Foolen, J., Janssen-van den Broek, M., Baaijens, F., 2014. Synergy between Rho signaling and matrix density in cyclic stretch-induced stress fiber organization. Acta Biomater. 10, 1876–1885.

Foolen, J., Deshpande, V., Kanters, F., Baaijens, F., 2012. The influence of matrix integrity on stress-fiber remodeling in 3D. Biomaterials 33, 7508–7518.

Gauvin, R., Parenteau-Bareil, R., Larouche, D., Marcoux, H., Bisson, F., Bonnet, A., Auger, F., Bolduc, S., Germain, L., 2011. Dynamic mechanical stimulations induce anisotropy and improve the tensile properties of engineered tissues produced without exogenous scaffolding. Acta Biomater. 7, 3294–3301.

Gérémie, L., Ilker, E., Bernheim-Dennery, M., Cavaniol, C., Viovy, J.-L., Vignjevic, D., Joanny, J.-F., Descroix, S., 2022. Evolution of a confluent gut epithelium under on-chip cyclic stretching. Phys. Rev. Res. 4, 023032.

Goldyn, A., Kaiser, P., Spatz, J., Ballestrem, C., Kemkemer, R., 2010. The kinetics of force-induced cell reorganization depend on microtubules and actin. Cytoskeleton 67, 241–250.

Goli-Malekabadi, Z., Tafazzoli-Shadpour, M., Rabbani, M., Janmaleki, M., 2011. Effect of uniaxial stretch on morphology and cytoskeleton of human mesenchymal stem cells: Static vs. Dynamic loading. Biomedizinische Technik 56, 259–265.

Greiner, A., Biela, S., Chen, H., Spatz, J., Kemkemer, R., 2015. Temporal responses of human endothelial and smooth muscle cells exposed to uniaxial cyclic tensile strain. Exp. Biol. Med. 240, 1298–1309.

Greiner, A., Chen, H., Spatz, J., Kemkemer, R., 2013. Cyclic tensile strain controls cell shape and directs actin stress fiber formation and focal adhesion alignment in spreading cells. PLoS One 8, e77328.

Harris, A., Wild, P., Stopak, D., 1980. Silicone rubber substrata: A new wrinkle in the study of cell locomotion. Science 208, 177–179.

Haston, W., Shields, J., Wilkinson, P., 1983. The orientation of fibroblasts and neutrophils on elastic substrata. Exp. Cell Res. 146, 117–126.

Hayakawa, K., Hosokawa, A., Yabusaki, K., Obinata, T., 2000. Orientation of smooth muscle-derived A10 cells in culture by cyclic stretching: Relationship between stress fiber rearrangement and cell reorientation. Zool. Sci. 17, 617–624.

Hayakawa, K., Sato, N., Obinata, T., 2001. Dynamic reorientation of cultured cells and stress fibers under mechanical stress from periodic stretching. Exp. Cell Res. 268, 104–114.

Hill, A., 1938. The heat of shortening and the dynamic constants of muscle. Proc. R. Soc. B 126, 136–195.

Holzapfel, G., Ogden, R., 2009. Constitutive modelling of passive myocardium: a structurally based framework for material characterization. Phil. Trans. R. Soc. A 367, 3445–3475.

Hsu, H.-J., Lee, C.-F., Kaunas, R., 2009. A dynamic stochastic model of frequency-dependent stress fiber alignment induced by cyclic stretch. PLoS One 4, e4853.

Hsu, H.-J., Lee, C.-F., Locke, A., Vanderzyl, S., Kaunas, R., 2010. Stretch-induced stress fiber remodeling and the activations of JNK and ERK depend on mechanical strain rate, but not FAK. PLoS One 5, e12470.

Hu, J.-J., Humphrey, J., Yeh, A., 2009. Characterization of engineered tissue development under biaxial stretch using nonlinear optical microscopy. Tissue Eng. A 15 (7), 1553–1564.

Huang, C., Miyazaki, K., Akaishi, S., Watanabe, A., Hyakusoku, H., Ogawa, R., 2013. Biological effects of cellular stretch on human dermal fibroblasts. J. Plast. Reconstr. Aesthetic Surg. 66, e351–e361.

Iba, T., Sumpio, B., 1991. Morphological response of human endothelial cells subjected to cyclic strain in vitro. Microvasc. Res. 42, 245–254.

Ingber, D., 2003. Mechanobiology and diseases of mechanotransduction. Ann. Med. 35, 564–577.

Ives, C., Eskin, S., McIntire, L., 1986. Mechanical effects on endothelial cell morphology: In vitro assessment. Vitro Cell. Dev. Biol. 22 (9), 500–507.

Iwaki, M., Ito, S., Morioka, M., Iwata, S., Numaguchi, Y., Ishii, M., Kondo, M., Kume, H., Naruse, K., Sokabe, M., Hasegawa, Y., 2009. Mechanical stretch enhances IL-8 production in pulmonary microvascular endothelial cells. Biochem. Biophys. Res. Commun. 389, 531–536.

Jungbauer, S., Gao, H., Spatz, J., Kemkemer, R., 2008. Two characteristic regimes in frequency-dependent dynamic reorientation of fibroblasts on cyclically stretched substrates. Biophys. J. 95, 3470–3478.

Kanda, K., Matsuda, T., 1993. Behavior of arterial wall cells cultured on periodically stretched substrates. Cell Transpl. 2, 475–484.

Kanda, K., Matsuda, T., 1994. Mechanical stress-induced orientation and ultrastructural change of smooth muscle cells cultured in three-dimensional collagen lattices. Cell Transpl. 3 (6), 481–492.

Kaunas, R., Hsu, H.-J., 2009. A kinematic model of stretch-induced stress fiber turnover and reorientation. J. Theoret. Biol. 257, 320–330.

Kaunas, R., Hsu, H.-J., Deguchi, S., 2011. Sarcomeric model of stretch-induced stress fiber reorganization. Cell Health Cytoskeleton 3, 13–22.

Kaunas, R., Nguyen, P., Usami, S., Chien, S., 2005. Cooperative effects of Rho and mechanical stretch on stress fiber organization. Proc. Natl. Acad. Sci. USA 102 (44), 15895–15900.

Kaunas, R., Usami, S., Chien, S., 2006. Regulation of stretch-induced JNK activation by stress fiber orientation. Cell. Signal. 18, 1924–1931.

Kemkemer, R., Jungbauer, S., Kaufmann, D., Gruler, H., 2006. Cell orientation by a microgrooved substrate can be predicted by automatic control theory. Biophys. J. (ISSN: 0006-3495) 90 (12), 4701–4711. http://dx.doi.org/10.1529/biophysj.105.067967, URL https://www.sciencedirect.com/science/article/pii/S0006349506726455.

Kemkemer, R., Neidlinger-Wilke, C., Claes, L., Gruler, H., 1999. Cell orientation induced by extracellular signals. Cell Biochem. Biophys. 30, 167–192.

Kim, B.-S., Nikolovski, J., Bonadio, J., Mooney, D., 1999. Cyclic mechanical strain regulates the development of engineered smooth muscle tissue. Nature Biotechnol. 17, 979–983.

Kong, F., Garcia, A., Mould, A., Humphries, M., Zhu, C., 2009. Demonstration of catch bonds between an integrin and its ligand. J. Cell Biol. 185, 1275–1284.

Kong, D., Ji, B., Dai, L., 2008. Stability of adhesion clusters and cell reorientation under lateral cyclic tension. Biophys. J. 95, 4034–4044.

Kreis, T., Geiger, B., Schlessinger, J., 1982. Mobility of micro-injected rhodamine actin within living chicken gizzard cells determined by fluorescence photobleaching recovery. Cell 29, 835–845.

Kumar, S., Maxwell, I., Heisterkamp, A., Polte, T., Lele, T., Salanga, M., Mazur, E., Ingber, D., 2006. Viscoelastic retraction of single living stress fibers and its impact on cell shape, cytoskeletal organization, and extracellular matrix mechanics. Biophys. J. 90, 3762–3773.

Kurpinski, K., Chu, J., Hashi, C., Li, S., 2006. Anisotropic mechanosensing by mesenchymal stem cells. Proc. Natl. Acad. Sci. USA 103 (44), 16095–16100.

Lazopoulos, K., Pirentis, A., 2007. Substrate stretching and reorganization of stress fibers as a finite elasticity problem. Int. J. Solids Struct. 44, 8285–8296.

Lazopoulos, K., Stamenovic, D., 2006. A mathematical model of cell reorientation in response to substrate stretching. MCB 3, 43–48.

Lee, C.-F., Haase, C., Deguchi, S., Kaunas, R., 2010. Cyclic stretch-induced stress fiber dynamics – Dependence on strain rate, Rho-kinase and MLCK. Biochem. Biophys. Res. Commun. 401, 344–349.

Lee, E., Holmes, J., Costa, K., 2008. Remodeling of engineered tissue anisotropy in response to altered loading conditions. Ann. Biomed. Eng. 36 (8), 1322–1334.

Lin, J., Li, X., Yin, J., Qian, J., 2020. Effect of cyclic stretch on neuron reorientation and axon outgrowth. Front. Bioeng. Biotechnol. 8, 597867.

Liu, B., Qu, M.-J., Qin, K.-R., Li, H., Li, Z.-K., Shen, B.-R., Jiang, Z.-L., 2008. Role of cyclic strain frequency in regulating the alignment of vascular smooth muscle cells in vitro. Biophys. J. 94, 1497–1507.

Livne, A., Bouchbinder, E., Geiger, B., 2014. Cell reorientation under cyclic stretching. Nature Commun. 5, 3938.

Loy, N., Preziosi, L., 2023. A Statistical Mechanics approach to describe cell re-orientation under stretch. Bulletin of Mathematical Biology 85, 60.

Lu, L., Feng, Y., Hucker, W., Oswald, S., Longmore, G., Yin, F.-P., 2008. Actin stress fiber pre-extension in human aortic endothelial cells. Cytoskeleton 65, 281–294.

Lucci, G., Giverso, C., Preziosi, L., 2021. Cell orientation under stretch: Stability of a linear viscoelastic model. Math. Biosci. 337, 108630.

Lucci, G., Preziosi, L., 2021. A nonlinear elastic description of cell preferential orientations over a stretched substrate. Biomech. Model. Mechanobiol. 20, 631–649.

Mao, T., He, Y., Gu, Y., Yang, Y., Yu, Y., Wang, X., Ding, J., 2021. Critical frequency and critical stretching rate for reorientation of cells on a cyclically stretched polymer in a microfluidic chip. AMS Appl. Mater. Interfaces 13, 13934–13948.

Mason, J., Ramseth, D., Chanter, D., Moon, T., Goodman, D., Mendzelevski, B., 2007. Electrocardiographic reference ranges derived from 79,743 ambulatory subjects. J. Electrocardiol. 40, 228–234.

Matheson, L., Fairbank, N., Maksym, G., Santerre, J., Labow, R., 2006. Characterization of the Flexcell™ Uniflex™ cyclic strain culture system with U937 macrophage-like cells. Biomaterials 27, 226–233.

Matsugaki, A., Fujiwara, N., Nakano, T., 2013. Continuous cyclic stretch induces osteoblast alignment and formation of anisotropic collagen fiber matrix. Acta Biomater. 9, 7227–7235.

Matsumoto, T., Delafontaine, P., Schnetzer, K., Tong, B., Nerem, R., 1996. Effect of uniaxial cyclic stretch on the morphology of monocytes/macrophages in culture. J. Biomech. Eng. 118, 420–422.

Matsumoto, T., Sasaki, J.-I., Alsberg, E., Egusa, H., Yatani, H., Sohmura, T., 2007. Three-dimensional cell and tissue patterning in a strained fibrin gel system. PLoS One 2, e1211.

McEvoy, E., Deshpande, V., McGarry, P., 2019. Transient active force generation and stress fibre remodelling in cells under cyclic loading. Biomech. Model. Mechanobiol. 18, 921–937.

Moretti, M., Prina-Mello, A., Reid, A., Barron, V., Prendergast, P., 2004. Endothelial cell alignment on cyclically-stretched silicone surfaces. J. Mater. Sci. Mater. Med. 15, 1159–1164.

Moriel, A., Livne, A., Bouchbinder, E., 2022. Cellular orientational fluctuations, rotational diffusion and nematic order under periodic driving. Soft Matter 18, 7091–7102.

Morioka, M., Parameswaran, H., Naruse, K., Kondo, M., Sokabe, M., Hasegawa, Y., Suki, B., Ito, S., 2011. Microtubule dynamics regulate cyclic stretch-induced cell alignment in human airway smooth muscle cells. PLoS One 6, e26384.

Morita, Y., Watanabe, S., Ju, Y., Yamamoto, S., 2013. In vitro experimental study for the determination of cellular axial strain threshold and preferential axial strain from cell orientation behavior in a non-uniform deformation field. Cell Biochem. Biophys. 67, 1249–1259.

Na, S., Meininger, G., Humphrey, J., 2007. A theoretical model for F-actin remodeling in vascular smooth muscle cells subjected to cyclic stretch. J. Theoret. Biol. 246, 87–99.

Nagatomi, J., Khashayar Toosi, K., Grashow, J., Chancellor, M., Sacks, M., 2005. Quantification of bladder smooth muscle orientation in normal and spinal cord injured rats. Ann. Biomed. Eng. 33 (8), 1078–1089.

Nagayama, K., Kimura, Y., Makino, N., Matsumoto, T., 2012. Strain waveform dependence of stress fiber reorientation in cyclically stretched osteoblastic cells: effects of viscoelastic compression of stress fibers. Am. J. Physiol. Cell Physiol. 302, C1469–C1478.

Neidlinger-Wilke, C., Grood, E., Claes, L., Brand, R., 2002. Fibroblast orientation to stretch begins within three hours. J. Orthop. Res. 20, 953–956.

Neidlinger-Wilke, C., Grood, E., Wang, J.H.-C., Brand, R., Claes, L., 2001. Cell alignment is induced by cyclic changes in cell length: studies of cells grown in cyclically stretched substrates. J. Orthop. Res. 19, 286–293.

Ngu, H., Feng, Y., Lu, L., Oswald, S., Longmore, G., Yin, F.C.-P., 2010. Effect of focal adhesion proteins on endothelial cell adhesion, motility and orientation response to cyclic strain. Ann. Biomed. Eng. 38, 208–222.

Niediek, V., Born, S., Hampe, N., Kirchgeßner, N., Merkel, R., Hoffmann, B., 2012. Cyclic stretch induces reorientation of cells in a Src family kinase- and p130Cas-dependent manner. Eur. J. Cell Biol. 91, 118–128.

Nieponice, A., Maul, T., Cumer, J., Soletti, L., Vorp, D., 2007. Mechanical stimulation induces morphological and phenotypic changes in bone marrow-derived progenitor cells within a three-dimensional fibrin matrix. J. Biomed. Mater. Res. A 81 (3), 523–530.

Obbink-Huizer, C., Oomens, C., Loerakker, S., Foolen, J., Bouten, C., Baaijens, F., 2014. Computational model predicts cell orientation in response to a range of mechanical stimuli. Biomech. Model. Mechanobiol. 13, 227–236.

Pettermann, H., Cheyrou, C., DeSimone, A., 2020. Modeling and simulation of anisotropic linear viscoelasticity. Mech. Time-Depend. Mater. 25, 679–689.

Pettermann, H., DeSimone, A., 2018. An anisotropic linear thermo-viscoelastic constitutive law. Mech. Time-Depend. Mater. 22, 877–890.

Pirentis, A., Peruski, E., Iordan, A., Stamenovic, D., 2011. A model for stress fiber realignment caused by cytoskeletal fluidization during cyclic stretching. Cell. Mol. Bioeng. 4, 67–80.

Qian, J., Liu, H., Lin, Y., Chen, W., Gao, H., 2013. A mechanochemical model of cell reorientation on substrates under cyclic stretch. PLoS One 8, e65864.

Reynolds, N., McEvoy, E., Panadero Perez, J., Coleman, R., McGarry, J., 2020. Influence of multi-axial dynamic constraint on cell alignment and contractility in engineered tissues. J. Mech. Behav. Biomed. Mater. 1112, 104024.

Rhodin, J., 1962. Fine structure of vascular walls in mammals, with special reference to smooth muscle component. Physiol. Rev. 42, 48–81.

Rihel, B., Park, J.-H., Kwon, I., Lim, J., 2012. Mechanical stretching for tissue engineering: Two-dimensional and three-dimensional constructs. Tissue Eng. B Rev. 18, 288–300.

Ristori, T., Vigliotti, A., Baaijens, F., Loerakker, S., Deshpande, V., 2016. Prediction of cell alignment on cyclically strained grooved substrates. Biophys. J. 111, 2274–2285.

Ritchie, A., Wijaya, S., Ong, W., Zhong, S., Chian, K., 2009. Dependence of alignment direction on magnitude of strain in esophageal smooth muscle cells. Biotechnol. Bioeng. 102 (6), 1703–1711.

Roshanzadeh, A., Nguyen, T., Nguyen, K., Kim, D.-S., Lee, B.-K., Lee, D.-W., Kim, E.-S., 2020. Mechanoadaptive organization of stress fiber subtypes in epithelial cells under cyclic stretches and stretch release. Sci. Rep. 10, 18684.

Rubbens, M., Driessen-Mol, A., Boerboom, R., Koppert, M., van Assen, H., Ter-Haar Romeny, B., Baaijens, F., Bouten, C., 2009. Quantification of the temporal evolution of collagen orientation in mechanically conditioned engineering cardiovascular tissues. Ann. Biomed. Eng. 37 (7), 1263–1272.

Safran, S., De, R., 2009. Nonlinear dynamics of cell orientation. Phys. Rev. E 80, 060901 (R).

Sato, K., Adachi, T., Matsuo, M., Tomita, Y., 2005. Quantitative evaluation of threshold fiber strain that induces reorganization of cytoskeletal actin fiber structure in osteoblastic cells. J. Biomech. 38, 1895–1901.

Schwarz, U., Safran, S., 2002. Elastic interactions of cells. Phys. Rev. Lett. 88, 048102.

Shikata, Y., Rios, A., Kawkitinarong, K., DePaola, N., Garcia, J., Birukov, K., 2005. Differential effects of shear stress and cyclic stretch on focal adhesion remodeling, site-specific FAK phosphorylation, and small GTPases in human lung endothelial cells. Exp. Cell Res. 304, 40–49.

Shirinsky, V., Antonov, A., Birukov, K., Sobolevsky, A., Romanov, Y., Kabaeva, N., Antonova, G., Smirnov, V., 1989. Mechano-chemical control of human endothelium orientation and size. J. Cell Biol. 109, 331–339.

Shishvan, S., Vigliotti, A., Deshpande, V., 2018. The homeostatic ensemble for cells. Biomech. Model. Mechanobiol. 17, 1631–1662.

Stamenovic, D., Lazopoulos, K., Pirentis, A., Suki, B., 2009. Mechanical stability determines stress fiber and focal adhesion orientation. Cell. Mol. Bioeng. 2, 475–485.

Standley, P., Camaratta, A., Nolan, B., Purgason, C., Stanley, M., 2002. Cyclic stretch induces vascular smooth muscle cell alignment via NO signaling. Am. J. Physiol. Heart Circul. Physiol. 283, H1907–H1914.

Sumpio, B., Banes, A., Link, W., Johnson, G., 1988. Enhanced collagen production by smooth muscle cells during repetitive mechanical stretching. Arch. Surg. 123, 1233–1236.

Takayama, A., Nagamine, T., Kotani, K., 2019. Aging is independently associated with an increasing normal respiratory rate among an older adult population in a clinical setting: A cross-sectional study. Geriatr. Gerontol. Int. 19, 1179–1183.

Takemasa, T., Sugimoto, K., Yamashita, K., 1997. Amplitude-dependent stress fiber reorientation in early response to cyclic strain. Exp. Cell Res. 230, 407–410.

Takemasa, T., Yamaguchi, T., Yamamoto, Y., Sugimoto, K., Yamashita, K., 1998. Oblique alignment of stress fibers in cells reduces the mechanical stress in cyclically deforming fields. Eur. J. Cell Biol. 77, 91–99.

Tamiello, C., Bouten, C., Baaijens, F., 2015. Competition bewteen cap and basal actin fiber orientation in cells subjected to contact guidance and cyclic strain. Sci. Rep. 5, 8752.

Tamiello, C., Buskermolen, A., Baaijens, F., Broers, J., Bouten, C., 2016. Heading in the right direction: Understanding cellular orientation responses to complex biophysical environments. Cell. Mol. Bioeng. 9, 12–37.

Terracio, L., Miller, B., Borg, T., 1988. Effects of cyclic mechanical stimulation of the cellular components of the heart: In vitro. Vitro Cell. Dev. Biol. 24 (1), 53–58.

Thodeti, C., Matthews, B., Ravi, A., Mammoto, A., Ghosh, K., Bracha, A., Ingber, D., 2009. TRPV4 channels mediate cyclic strain-induced endothelial cell reorientation through integrin-to-integrin signaling. Circ. Res. 104, 1123–1130.

Throm Quinlan, A., Sierad, L., Capulli, A., Firstenberg, L., Billiar, K., 2011. Combining dynamic stretch and tunable stiffness to probe cell mechanobiology in vitro. PLoS One 6, e23272.

Tojkander, S., Gateva, G., Lappalainen, P., 2012. Actin stress fibers - assembly, dynamics and biological roles. J. Cell Sci. 125, 1855–1864.

Tondon, A., Hsu, H.-J., Kaunas, R., 2012. Dependence of cyclic stretch-induced stress fiber reorientation on stretch waveform. J. Biomech. 45, 728–735.

Tondon, A., Kaunas, R., 2014. The direction of stretch-induced cell and stress fiber orientation depends on collagen matrix stress. PLoS One 9, e89592.

Tulloch, N., Muskheli, V., Razumova, M., Korte, F., Regnier, M., Hauch, K., Pabon, L., Reinecke, H., Murry, C., 2011. Growth of engineered human myocardium with mechanical loading and vascular coculture. Circ. Res. 109, 47–59.

Ujihara, Y., Nakamura, M., Soga, M., Koshiyama, K., Miyazaki, H., Wada, S., 2015. Computational studies on strain transmission from a collagen gel construct to a cell and its internal cytoskeletal filaments. Comput. Biol. Med. 56, 20–29.

Vernerey, F., Farsad, M., 2011. A constrained mixture approach to mechano-sensing and force generation in contractile cells. J. Mech. Behav. Biomed. Mater. 4, 1683–1699.

Vigliotti, A., McMeeking, R., Deshpande, V., 2015. Simulation of the cytoskeletal response of cells on grooved or patterned substrates. J. R. Soc. Interface 12, 20141320.

Vigliotti, A., Ronan, W., Baaijens, F., Deshpande, V., 2016. A thermodynamically motivated model for stress-fiber reorganization. Biomech. Model. Mechanobiol. 15, 761–789.

Wakatsuki, T., Elson, E., 2003. Reciprocal interactions between cells and extracellular matrix during remodeling of tissue constructs. Biophys. Chem. 100, 593–605.

Wang, J.H.-C., 2000. Substrate deformation determines actin cytoskeleton reorganization: A mathematical modeling and experimental study. J. Theoret. Biol. 202, 33–41.

Wang, J.H.-C., Goldschmidt-Clermont, P., Wille, J., Yin, F.C.-P., 2001. Specificity of endothelial cell reorientation in response to cyclic mechanical stretching. J. Biomech. 34, 1563–1572.

Wang, J.H.-C., Goldschmidt-Clermont, P., Yin, F.C.-P., 2000. Contractility affects stress fiber remodeling and reorientation of endothelial cells subjected to cyclic mechanical stretching. Ann. Biomed. Eng. 28, 1165–1171.

Wang, J.H.-C., Grood, E., 2000. The strain magnitude and contact guidance determine orientation response of fibroblasts to cyclic substrate strains. Connect. Tissue Res. 41 (1), 29–36.

Wang, H., Ip, W., Boissy, R., Grood, E., 1995. Cell orientation response to cyclically deformed substrates: experimental validation of a cell model. J. Biomech. 28 (12), 1543–1552.

Wang, S., Lu, D., Zhang, Z., Jia, X., Yang, L., 2018. Effects of mechanical stretching on the morphology of extracellular polymers and the mRNA expression of collagens and small leucine-rich repeat proteoglycans in vaginal fibroblasts from women with pelvic organ prolapse. PLoS One 13, e0193456.

Wang, S., Zhang, Z., Lu, D., Xu, Q., 2015. Effects of mechanical stretching on the morphology and cytoskeleton of vaginal fibroblasts from women with pelvic organ prolapse. Int. J. Mol. Sci. 16, 9406–9419.

Wei, Z., Deshpande, V., McMeeking, R., Evans, A., 2008. Analysis and interpretation of stress fiber organization in cells subject to cyclic stretch. J. Biomech. Eng. 130, 031009-1–031009-9.

White, G., Gimbrone, Jr., M., Fujiwara, K., 1983. Factors influencing the expression of stress fibers in vascular endothelial cells in situ. J. Cell Biol. 97, 416–424.

Wille, J., Ambrosi, C., Yin, F.C.-P., 2004. Comparison of the effects of cyclic stretching and compression of endothelial cell morphological responses. J. Biomech. Eng. 126, 545–551.

Wille, J., Elson, E., Okamoto, R., 2006. Cellular and matrix mechanics of bioartificial tissues during continuous cyclic stretch. Ann. Biomech. Eng. 34 (11), 1678–1690.

Wong, A., Pollard, T., Herman, I., 1983. Actin filament stress fibers in vascular endothelial cells in vivo. Science 219, 867–869.

Xu, G., Feng, X., Gao, H., 2018. Orientations of cells on compliant substrates under biaxial stretches: A theoretical study. Biophys. J. 114, 701–710.

Xu, G., Li, B., Feng, X., Gao, H., 2016. A tensegrity model of cell reorientation on cyclically stretched substrates. Biophys. J. 111, 1478–1486.

Yamane, M., Matsuda, T., Ito, T., Fujio, Y., Takahashi, K., Azuma, J., 2007. Rac1 activity is required for cardiac myocyte alignment in response to mechanical stress. Biochem. Biophys. Res. Commun. 353, 1023–1027.

Yoshigi, M., Clark, E., Yost, H., 2003. Quantification of stretch-induced cytoskeletal remodeling in vascular endothelial cells by image processing. Cytom. A 55A, 109–118.

Zemel, A., Bischofs, I., Safran, S., 2006. Active elasticity of gels with contractile cells. Phys. Rev. Lett. 97, 128103.

Zhang, L., Kahn, C., Chen, H.-Q., Tran, N., Wang, X., 2008. Effect of uniaxial stretching on rat bone mesenchymal stem cell: Orientation and expressions of collagen types I and III and tenascin-C. Cell Biol. Int. 32, 344–352.

Zhao, S., Suciu, A., Ziegler, T., Moore, J., Bürki, E., Meister, J.-J., Brunner, H., 1995. Synergistic effects of fluid shear stress and cyclic circumferential stretch on vascular endothelial cell morphology and cytoskeleton. Arterioscler. Thromb. Vasc. Biol. 15, 1781–1786.

Zhong, Y., Kong, D., Dai, L., Ji, B., 2011. Frequency-dependent focal adhesion instability and cell reorientation under cyclic substrate stretching. Cell. Mol. Bioeng. 4, 442–456.

Zhu, J.-H., Chen, C.-L., Flavahan, S., Harr, J., Su, B., Flavahan, N., 2011. Cyclic stretch stimulates vascular smooth muscle cell alignment by redox-dependent activation of Notch3. Am. J. Physiol. Heart Circul. Physiol. 300, H1770–H1780.

Zielinski, A., Linnartz, C., Pleschka, C., Dreissen, G., Springer, R., Merkel, R., Hoffmann, B., 2018. Reorientation dynamics and structural interdependencies of actin, microtubules and intermediate filaments upon cyclic stretch application. Cytoskeleton 75, 385–394.